

Current Star Formation in the Ophiuchus and Perseus Molecular Clouds: Constraints and Comparisons from Unbiased Submillimeter and Mid-Infrared Surveys. II.

Jes K. Jørgensen^{1,2,*}, Doug Johnstone^{3,4}, Helen Kirk^{4,3}, Philip C. Myers¹, Lori E. Allen¹, & Yancy L. Shirley⁵

ABSTRACT

We present a census of the population of deeply embedded young stellar objects (YSOs) in the Ophiuchus molecular cloud complex based on a combination of Spitzer Space Telescope mid-infrared data from the “Cores to Disks” (c2d) legacy team and JCMT/SCUBA submillimeter maps from the COMPLETE team. We have applied a method developed for identifying embedded protostars in Perseus to these datasets and in this way construct a relatively unbiased sample of 27 candidate embedded protostars with envelopes more massive than our sensitivity limit (about $0.1 M_{\odot}$). As in Perseus, the mid-infrared sources are located close to the center of the SCUBA cores and the narrowness of the spatial distribution of mid-infrared sources around the peaks of the SCUBA cores suggests that no significant dispersion of the newly formed YSOs has occurred. Embedded YSOs are found in 35% of the SCUBA cores - less than in Perseus (58%). On the other hand the mid-infrared sources in Ophiuchus have less red mid-infrared colors, possibly indicating that they are less embedded. We apply a nearest neighbour surface density algorithm to define the substructure in each of the clouds and calculate characteristic numbers for each subregion - including masses, star formation efficiencies, fraction of embedded sources etc. Generally the main clusters in Ophiuchus and Perseus (L1688, NGC1333 and IC 348) are found to have higher star formation efficiencies than small groups such as

¹Harvard-Smithsonian Center for Astrophysics, 60 Garden Street MS42, Cambridge, MA 02138, USA

²Argelander-Institut für Astronomie, University of Bonn, Auf dem Hügel 71, 53121, Bonn, Germany

³Herzberg Institute of Astrophysics, National Research Council of Canada, 5071 West Saanich Road, Victoria, BC V9E 2E7, Canada

⁴Department of Physics & Astronomy, University of Victoria, Victoria, BC, V8P 1A1, Canada

⁵Bart J. Bok Fellow, Steward Observatory, University of Arizona, 933 N. Cherry Ave., Tucson, AZ 85721

*Current address: Argelander-Institut für Astronomie. E-mail: jes@astro.uni-bonn.de

B1, L1455 and L1448, which on the other hand are completely dominated by deeply embedded protostars. We discuss possible explanations for the differences between the regions in Perseus and Ophiuchus, such as different evolutionary timescales for the YSOs or differences, e.g., in the accretion in the two clouds.

Subject headings: stars: formation — ISM: clouds — ISM: evolution — stars: pre-main sequence — ISM: individual (Ophiuchus, Perseus)

1. Introduction

Although the most detailed theoretical models of star formation continue to concentrate on the formation of an isolated star within a relatively pristine environment, these solutions are far removed from the conditions under which a vast majority of stars begin life. Stars form in environments which have a wide range of physical conditions, including large scale clusters containing high-mass stars, small groups of predominantly low-mass stars, and even the occasional isolated single star or binary. Relating the distribution of the pre- and protostellar cores to their environment on large scales is an important step toward understanding the global properties of stars such as the stellar initial mass function and the evolution process through the different stages of young stellar objects. It is therefore important to perform unbiased censuses of objects throughout their evolutionary stages. To date, the hardest sample to quantify has been the most deeply embedded stages where signatures of the object are observed in the mid- to far-infrared and submillimeter wavelengths.

In a previous paper (Jørgensen et al. 2007) we performed a detailed comparison between the *SCUBA* submillimeter dust continuum and *Spitzer Space Telescope* mid-infrared observations of sources in the Perseus molecular cloud in order to identify and examine the properties of starless cores and deeply embedded protostars. In this paper we extend the SCUBA and Spitzer analysis to Ophiuchus. We then use this analysis for a direct comparison between the Ophiuchus and Perseus clouds, paying particular attention to the global star formation and clustering properties of the clouds.

Previous studies of the deeply embedded stages have been hampered by low sensitivity single element (sub)millimeter receivers and confusion in low resolution, low sensitivity infrared observations such as those from the IRAS and ISO satellites. In the last few years systematic, detailed surveys of larger regions have been made possible using wide area imaging at high resolution and sensitivity using submillimeter telescopes such as the JCMT with SCUBA and mid-infrared telescopes including Spitzer and its Infrared Array Camera (*IRAC*) and Multiband Imaging Photometer (*MIPS*). The “Cores to Disks (c2d)”

Spitzer legacy team (Evans et al. 2003) mapped five of the nearby star forming clouds, including Perseus (Jørgensen et al. 2006; Rebull et al. 2007) and Ophiuchus (Padgett et al. 2008), using the Spitzer cameras. At submillimeter wavelengths the “COMPLETE” team (Goodman et al. 2004; Ridge et al. 2006) created maps of Perseus (Kirk et al. 2006) and Ophiuchus (Johnstone et al. 2004) at submillimeter wavelengths. Both these surveys compiled systematic samples of sources in an unbiased sense and together they provide excellent constraints on the properties of the starless cores and deeply embedded protostars in these cloud complexes.

Jørgensen et al. (2007) discussed how to associate mid-infrared Spitzer sources with submillimeter SCUBA cores: a characteristic population of mid-infrared sources were found closely associated with the centers of the SCUBA cores. These mid-infrared sources were furthermore found to have particularly red colors while the associated SCUBA cores were found to have high “concentrations”, i.e., appear centrally peaked. Determining whether this result is a discriminant of the earliest stage of star formation in general, or whether it is region specific, requires exploring additional clouds.

The construction of a relatively unbiased samples of embedded protostars, furthermore makes it possible to address some of the important questions concerning low-mass star formation and the relation between protostars and their environment. Based on the analysis of the Perseus data, Jørgensen et al. for example found that the Spitzer sources were strongly centered around the peaks of the submillimeter cores, suggesting that little dispersal of the newly formed YSOs relative to their parental cores occurs during the protostellar stages. Jørgensen et al. also found similar numbers of SCUBA cores with and without associated MIPS sources suggesting that the timescale for the evolution through the dense pre-stellar stages (where the cores are recognized in the SCUBA maps) is similar to the timescale for the evolution through the embedded protostellar stages. It is interesting to utilize a similar method to explore the similarities and differences between clouds and shed light onto the recent star formation history in different cloud environments.

The Ophiuchus molecular cloud complex¹ provides an excellent comparison to Perseus: Ophiuchus is similar to Perseus in the sense that it contains both embedded protostars and a similar number of SCUBA cores. In Perseus the population of young stellar objects can be divided into three main groups: the IC 348 cluster region mainly containing more evolved YSOs, the NGC 1333 region which is a more currently active cluster and the remainder, or extended cloud, which contains a handful of smaller groups, each with ~ 10 members and

¹Following the other c2d studies of Ophiuchus (Young et al. 2006; Padgett et al. 2008) a distance of 125 ± 25 pc (de Geus et al. 1989, see also discussion in Wilking et al. 2008) is adopted throughout this paper.

with a relatively high fraction of deeply embedded low-mass protostars compared to more evolved YSOs. The Ophiuchus cloud in contrast is dominated by the L1688 cluster with some, but significantly less, star formation occurring outside this main region. Comparing the embedded populations of YSOs, the distribution of cores and dust extinction between these two clouds, and their subgroups, makes it possible to test scenarios for star formation, and their robustness across differing environments.

This paper follows the approach of Jørgensen et al. (2007) and compares SCUBA submillimeter and Spitzer mid-infrared observations of the Ophiuchus molecular cloud. The paper is laid out as follows: §2 presents an overview of the submillimeter and mid-infrared data which forms the basis for this analysis. §3 applies the method from Jørgensen et al. (2007) to the Ophiuchus dataset. §4 presents an analysis of the substructure of Ophiuchus and Perseus using a nearest neighbor surface density algorithm and compares the key numbers for the two clouds and the subregions within them. §5 discusses the implications for star formation scenarios in the two clouds.

2. Observations: Large-scale maps of Ophiuchus

As in Jørgensen et al. (2007) the bases for this analysis are large scale maps of Ophiuchus at mid-infrared wavelengths with the *Spitzer Space Telescope* and at submillimeter wavelengths with the *SCUBA* bolometer array on the *JCMT*. In this section we present a brief discussion of the data, in particular highlighting differences with respect to the data presented in Jørgensen et al. (2007).

2.1. Submillimeter observations from JCMT/SCUBA

The *Submillimetre Common-User Bolometer Array (SCUBA)* on the *James Clerk Maxwell Telescope (JCMT)* mapped the cloud in 850 μm dust continuum emission at 15'' resolution as previously presented by Johnstone et al. (2004). For the present analysis these data were re-reduced and combined with all other SCUBA archive data for Ophiuchus following the description in Kirk et al. (2006) (see also Di Francesco et al. 2008). As with the Perseus data presented in Kirk et al. (2006), the standard SCUBA pipeline reduction was augmented by a matrix inversion image recreation procedure (Johnstone et al. 2000a). The resulting 3'' pixel images were smoothed on small scales by a Gaussian with dispersion of 3'' to remove pixel-to-pixel noise. Furthermore the maps were flattened by removing a large-scale Gaussian with dispersion of 90''. The resulting RMS of the map was about 0.03 Jy beam⁻¹. From

these maps, lists of cores were extracted using the 2D version of the Clumpfind algorithm (Williams et al. 1994) as described by Kirk et al. (2006) using a contouring level with a spacing, $\sigma = 0.03 \text{ Jy beam}^{-1}$ ($0.04 \text{ Jy beam}^{-1}$ in the Western part of the map around the Oph A core and around L1709). Only peaks above 5σ are reported. In this fashion 66 SCUBA cores were identified across the Ophiuchus field. We summarize the properties of cores in the appendix to this paper (see also the comparison to previous studies in Sect. 3.4).

2.2. Mid-infrared observations from *Spitzer*

Together with five other nearby star forming regions, Ophiuchus was mapped at 3.6, 4.5, 5.8, 8.0, 24, 70 and 160 μm using the *Spitzer Space Telescope's* IRAC and MIPS cameras by c2d (Padgett et al. 2008; Allen et al. 2008) identifying more than 600,000 sources with a signal-to-noise ratio of 3 or more in at least one of the 3.6–70 μm bands over an area of 12.2 degree². In total the SCUBA map covers approximately 5.7 degree² whereas the overlapping area between the IRAC and MIPS data covers 6.3 degree². In contrast to Perseus where the full area (3.6 degree²) of the SCUBA map is covered by the Spitzer observations, only about 80% of the SCUBA map of Ophiuchus (4.6 degree²) was covered by the Spitzer observations. No SCUBA cores were found outside this overlap region, however. Fig. 1 shows the SCUBA dust continuum emission overlaid as contours on Spitzer images of Ophiuchus and Perseus. Fig. 2 shows finding charts with the distribution of SCUBA cores and Spitzer mid-infrared sources in selected regions of Ophiuchus.

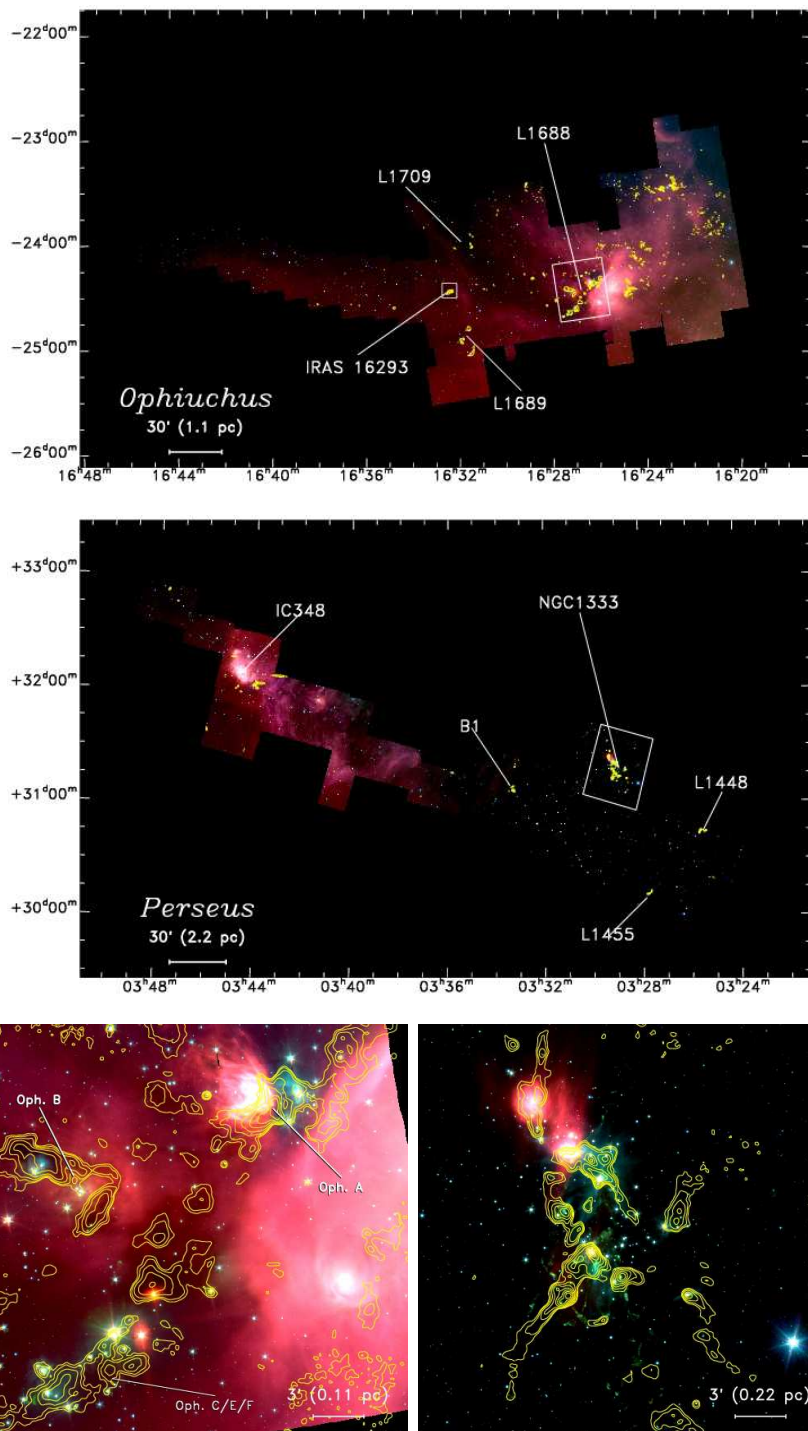


Fig. 1.— Three-color image (blue: IRAC1 $3.6 \mu\text{m}$, green: IRAC2 $4.5 \mu\text{m}$ and red: IRAC4 $8.0 \mu\text{m}$) overviews of the Ophiuchus and Perseus clouds with the main regions discussed in the text indicated. The lower panels show blow-ups of the L1688 region in Ophiuchus (left) and NGC 1333 region in Perseus (right). The yellow contours show the SCUBA $850 \mu\text{m}$ emission from the maps of Johnstone et al. (2004) and Kirk et al. (2006). The contours are shown at 9 logarithmically spaced levels between 40 mJy and 6 Jy. For a similar blow-up of the IRAS 16293 region see Fig. 8. For further details about the IRAC observations see Jørgensen et al. (2006) and Allen et al. (2008).

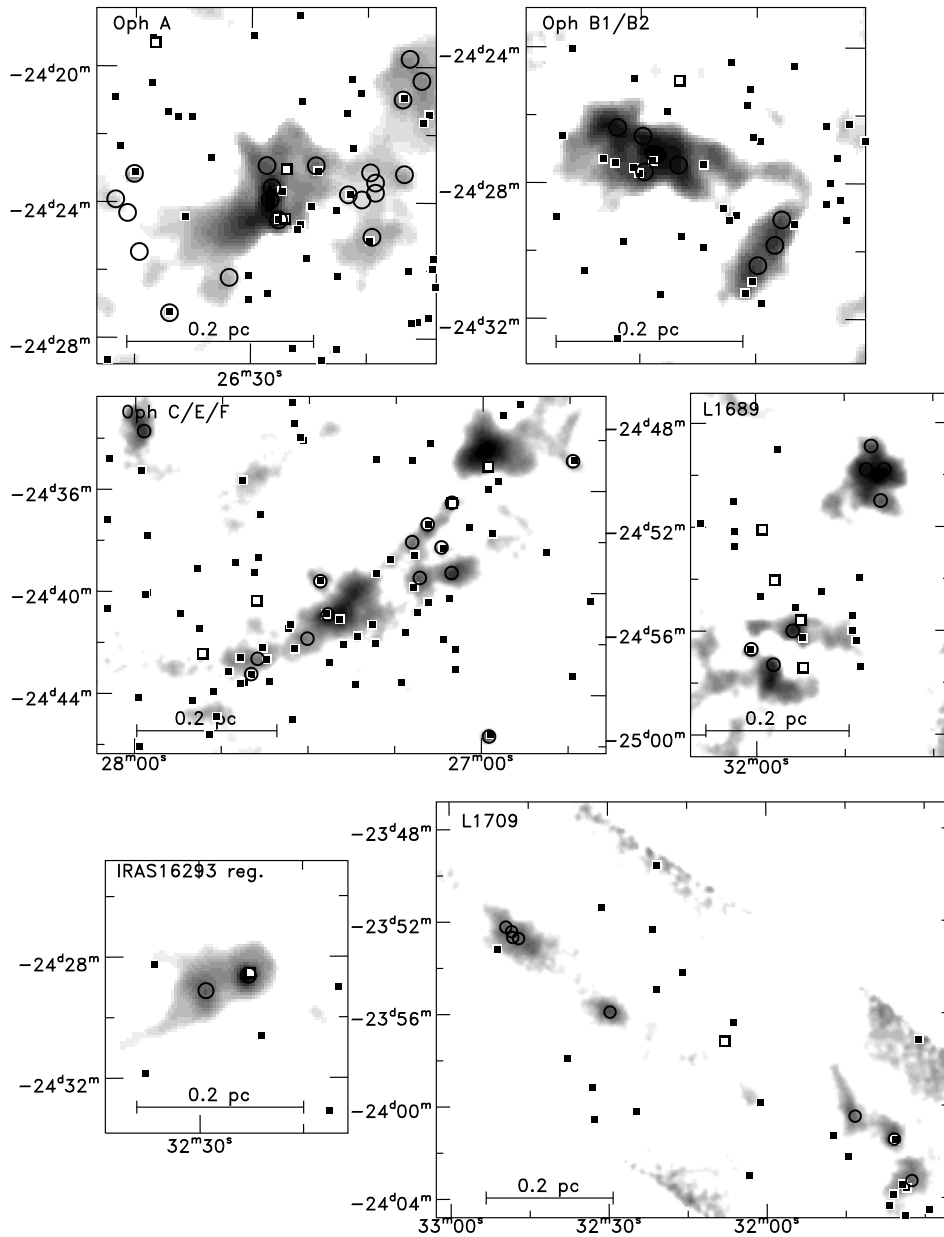


Fig. 2.— Finding charts for the Ophiuchus cloud. The SCUBA cores (circles) and MIPS $24 \mu\text{m}$ detected sources (filled squares) are plotted over SCUBA maps of six of the most prominent star forming regions indicated in Fig. 1. The sizes of the symbols of the SCUBA cores correspond to radii of $15''$ (twice the SCUBA Beam). The MIPS $24 \mu\text{m}$ detected sources with $[3.6] - [4.5] > 1.0$ and $[8.0] - [24] > 4.5$ are singled out with open squares.

Slight differences exist in the processing of the current (and final) c2d catalogs compared to the version that was used for analysis of Perseus in Jørgensen et al. (2007). Since that paper, all the c2d data were reprocessed using the SSC pipeline version S13. In the earlier catalogs, sources were extracted from the IRAC and MIPS 24 μm mosaics individually and the lists of sources from these catalogs *band-merged* as described in Evans et al. (2007). In the final catalogs delivered by c2d², this procedure has been improved by *band-filling* individual sources. That is, for sources without counterparts at one or more wavelengths, those mosaics were reexamined and a best attempt made to extract a source. However, for detection purposes sources are potentially suspect: for example outflow knots close to embedded protostars are easily picked up toward the PSF wings of the MIPS 24 μm detections of embedded YSOs and we therefore exclude them in the remainder of the analysis.

Another addition to the c2d processing, is bandmerging with observations at 70 μm . In this paper, we include sources that are either detected at 24 μm (excluding band-filled sources) or 70 μm as the basis for the analysis (in the following we refer to those sources as “MIPS sources”). This is in contrast to Jørgensen et al. (2007) where only the 24 μm catalogs were utilized. As we return to below, this procedure solves the problem that some well-known YSOs are saturated at 24 μm , an issue which was dealt with in Jørgensen et al. (2007) by including SCUBA cores with high concentrations.

2.3. Background contamination

Using this first cut of MIPS 24 μm detected sources we can also address the issue of background contamination: one of the complications in large scale mappings such as those presented in c2d is separating background contamination from the sample of candidate YSOs in an accurate statistical manner. This in particular means separating background galaxies from the sample of YSOs since both show similar red colors at mid-infrared wavelengths (see, e.g., Porras et al. 2007, for an illustrative example and discussion of this issue). For Perseus, Jørgensen et al. (2007) found that the density of MIPS 24 μm detected sources were low enough that the chance alignment between such a source and a SCUBA core was statistically small. This fact holds true as well for Ophiuchus: with 1325 MIPS 24 μm detected sources over 4.6 degree² we only find 0.08 sources within any 1 arcmin². This translates to a 1.5% chance of having a MIPS 24 μm source randomly aligned within a 15'' radius (one SCUBA half-power beam-width) of the center a given SCUBA core (or put in another way, statistically there will be 1 randomly assigned candidate in total within 15'' of

²Available at <http://ssc.spitzer.caltech.edu/legacy/c2dhistory.html>.

the 66 SCUBA cores in Ophiuchus).

3. Mid-infrared sources associated with dense cores

3.1. Constructing a sample of embedded protostars

Fig. 3 shows the distribution of MIPS sources with respect to the nearest submillimeter core for both Ophiuchus and Perseus. Sources with red mid-infrared colors ($[3.6] - [4.5] > 1.0$ and $[8.0] - [24] > 4.5$) are highlighted to reveal their high degree of correlation with the centers of SCUBA cores. Figs. 4 and 5 show the one dimensional distributions of $[3.6] - [4.5]$ and $[8.0] - [24]$ colors as a function of distance to the nearest SCUBA core. Both figures reveal that there is some clustering of the Ophiuchus sources relative to the core center, but with less significance than in Perseus. In Perseus the ratio of sources with $[3.6] - [4.5] > 1.0$ relative to those with $[3.6] - [4.5] \leq 1.0$ is 5.7 within $15''$ compared to 0.40 at distances of $30''$ – $60''$. In Ophiuchus the numbers are 1.5 and 0.53, respectively. That is, the number of red sources in SCUBA cores is about a factor 3.5–4 higher in Perseus than Ophiuchus. Furthermore, in Perseus, sources with significantly redder colors are found: 10 sources are found with $[3.6] - [4.5] > 2.5$ with a maximum of 4.4 whereas none this red are found in Ophiuchus. This difference between the redness of the embedded sources in Perseus vs. Ophiuchus may suggest a difference in their physical properties (see §5.3).

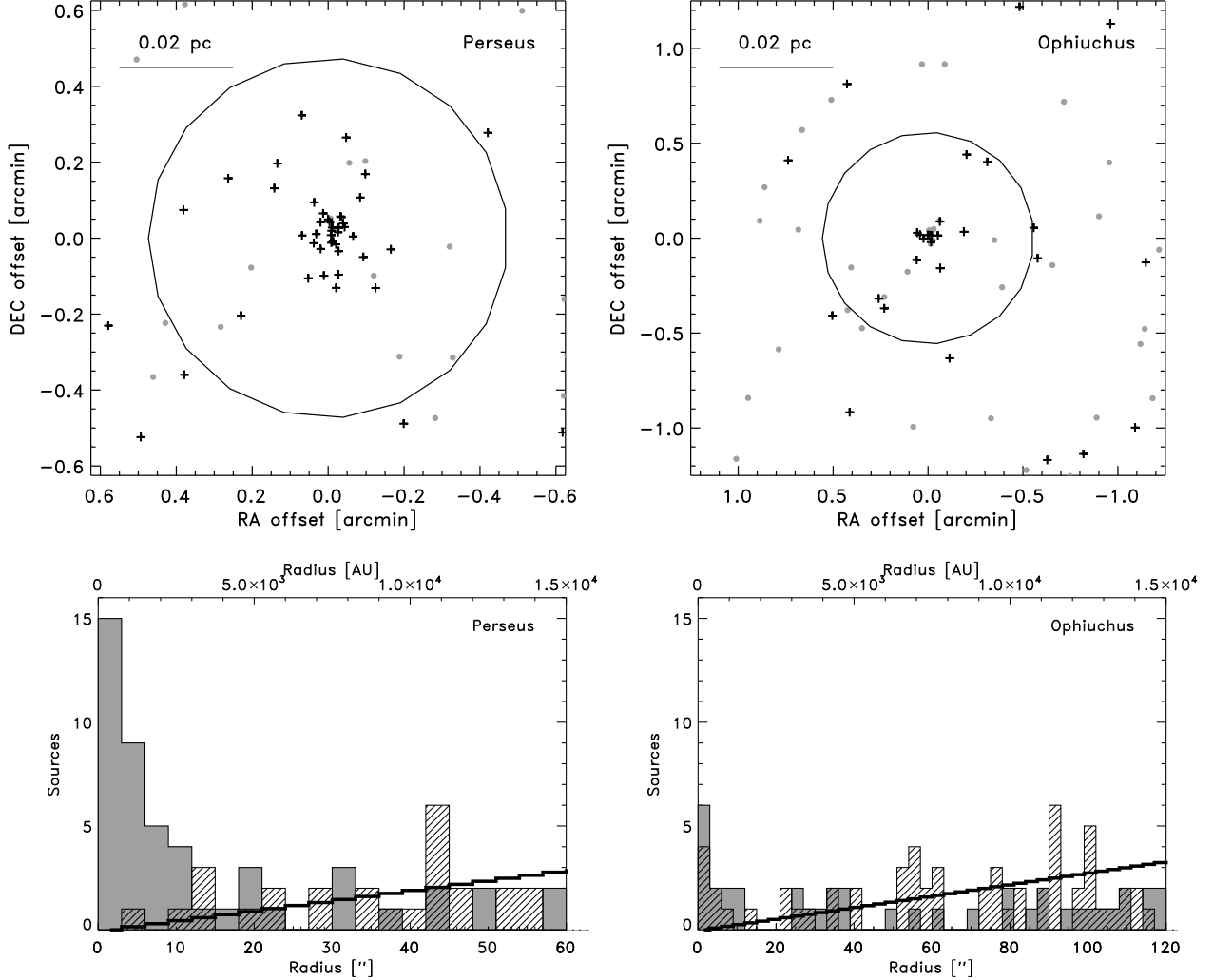


Fig. 3.— *Upper panels:* Distribution of MIPS sources with red mid-infrared colors ($[3.6] - [4.5] > 1.0$ and $[8.0] - [24] > 4.5$; black plus signs) compared to other MIPS sources (grey circles) around each SCUBA core (shifted to the same center). The size scales in the two plots are stretched to represent the same linear scale. The circle indicates the mean SCUBA core sizes. *Lower panels:* distribution of number of mid-infrared sources as a function of distance to the nearest SCUBA core. Again the filled grey histogram indicates the distribution of sources with $[3.6] - [4.5] > 1.0$ and $[4.5] - [8.0] > 4.5$ and the hatched histogram the distribution of the other sources. The thick black line indicates the prediction from a uniform source distribution with the same surface density as the observed distribution.

To establish samples of embedded YSOs we utilize these results to apply the same procedure Jørgensen et al. (2007) used on the Perseus datasets. In this paper we refer to embedded YSOs as any MIPS source (i.e., a source detected at either 24 or 70 μm) which is associated with a submillimeter core as traced by emission in the SCUBA maps or which fulfills certain color criteria (see below). Neither the mid-infrared source lists nor the submillimeter core identifications by themselves can be used unambiguously to define a sample of embedded objects, but as demonstrated in Jørgensen et al. (2007) they can be used in conjunction to form a relatively unbiased list of YSOs complete down to the resolution of the mid-infrared data. The three criteria developed for identifying candidate protostars in Perseus were based on the mid-infrared colors of Spitzer sources, associations between Spitzer sources and submillimeter cores and the concentration³ of SCUBA cores. In summary the list of embedded objects were constructed by selecting:

- A.** MIPS 24 μm catalog sources with $[3.6] - [4.5] > 1$ and $[8.0] - [24] > 4.5$, *or*
- B.** MIPS 24 μm catalog sources with distances less than 15'' to their nearest submillimeter core, *or*
- C.** Submillimeter cores with concentrations higher than 0.6.

The first criterion selects the most deeply embedded YSOs with steeply increasing SEDs but misses sources that are not detected in IRAC bands 1 or 2 - either due to confusion with outflows or simply because they in fact are very deeply embedded. The second criterion selects all MIPS sources that are embedded YSOs in the sense that they are located within two SCUBA beam sizes of a SCUBA core. That list will also include sources which are not necessarily directly associated with an observed submillimeter core due to confusion in the submillimeter map, poorly defined core structure, or the limiting sensitivity of the submillimeter observations. In Perseus it was found that most of the sources selected according to the second criterion also obeyed the first (upper panels of Fig. 4 and 5).

These first two criteria were found to still miss sources saturated at 24 μm . Such sources were selected by the third criterion, which did not in itself include all the mid-infrared sources under **A** and **B** (see Jørgensen et al. (2007)). On the other hand it was also shown that a number of low concentration cores in fact had embedded YSOs, so criterion **C** in itself was also not optimal for picking out candidate embedded YSOs. In contrast to Perseus, there

³The concentration of a SCUBA core is defined as $C = 1 - \frac{1.13 B^2 S_{850}}{(\pi R_{\text{obs}}^2 f_0)}$, where B is the beam size, S_{850} the total flux from the SCUBA observations at 850 μm , R_{obs} the measured radius and f_0 the peak flux (Johnstone et al. 2000b).

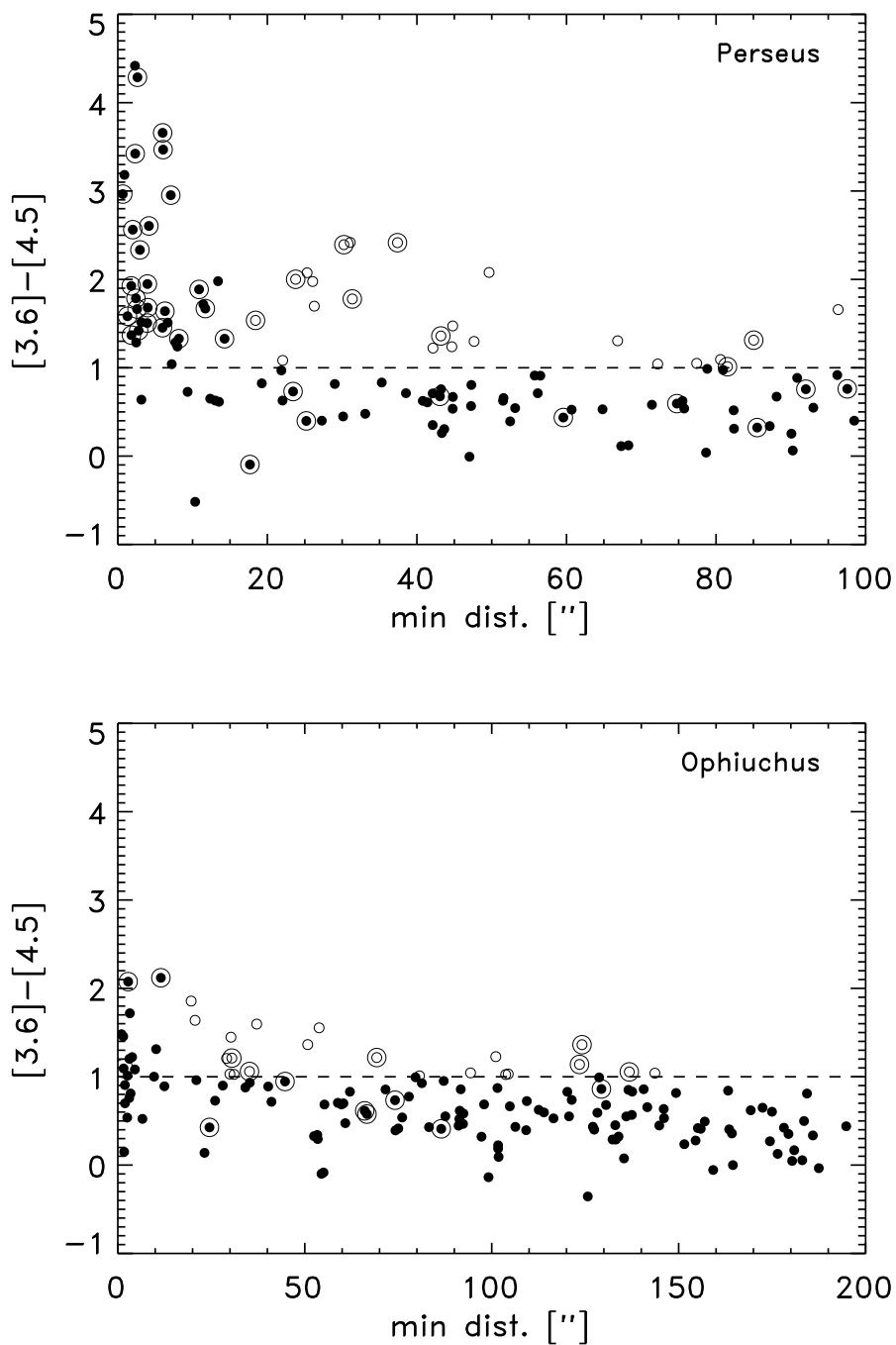


Fig. 4.— $[3.6] - [4.5]$ color of each MIPS source vs. its distance to the nearest submillimeter core. Upper panel for Perseus and lower panel for Ophiuchus. Sources are shown with filled circles except those with distances larger than $15''$ to their nearest cores and $[3.6] - [4.5] > 1.0$, which have been indicated by small open circles. Symbols (filled or open circles) with an extra larger circle around indicate mid-infrared sources with $[8.0] - [24]$ colors greater than 4.5.

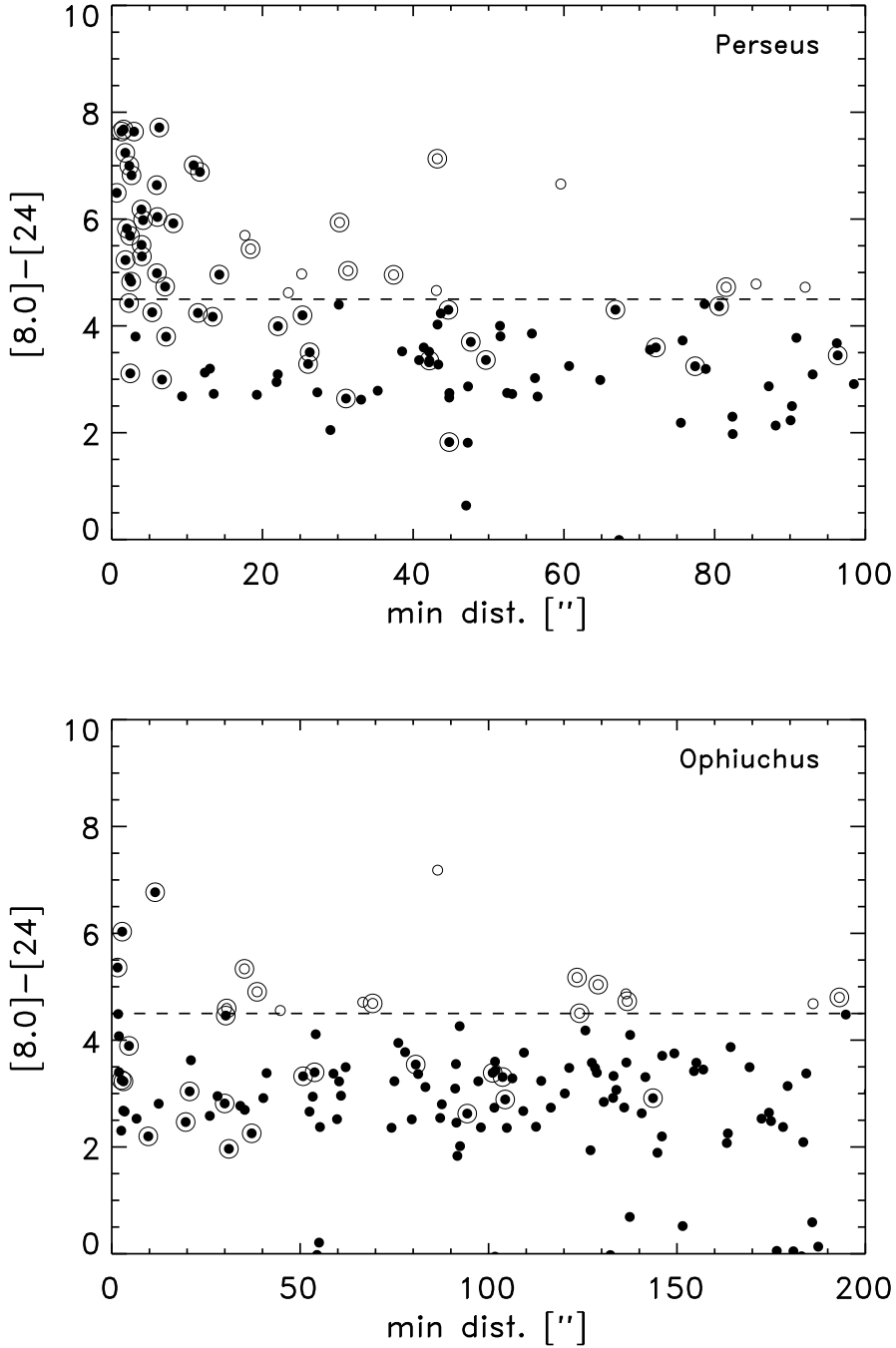


Fig. 5.— $[8.0] - [24]$ color of each MIPS source vs. its distance to the nearest submillimeter core. Upper panel for Perseus and lower panel for Ophiuchus. Sources are shown with filled circles except those with distances larger than $15''$ to their nearest cores and $[8.0] - [24] > 4.5$, which have been indicated by open circles. Symbols (filled or open circles) with an extra larger circle around indicate mid-infrared sources with $[3.6] - [4.5]$ colors greater than 1.0.

are a few cores with high concentrations ($C > 0.6$) in Ophiuchus that in fact are starless. As well, a few sources associated with lower concentration cores are found to be saturated at $24\ \mu\text{m}$ and therefore would not make it onto the list of protostars.

Visual inspection of all SCUBA cores, however, reveals that by adding sources that are detected at $70\ \mu\text{m}$, provides a sample of all the MIPS sources in Ophiuchus associated with SCUBA cores, even those clearly saturated or confused at $24\ \mu\text{m}$. This method can also be directly applied to Perseus: the four sources that were associated with high concentration cores all only have $70\ \mu\text{m}$ detections, whereas no new sources are added by utilizing this criterion in Perseus. In this way there is no need to rely on the observed empirical properties of the SCUBA cores⁴. Therefore, the two criteria required to identify candidate protostars in this paper in either Perseus or Ophiuchus are:

- A.** MIPS 24 or $70\ \mu\text{m}$ catalog sources with $[3.6] - [4.5] > 1$ and $[8.0] - [24] > 4.5$, *or*
- B.** MIPS 24 or $70\ \mu\text{m}$ catalog sources with distances less than $15''$ to their nearest core.

In this way a sample of 27 embedded YSOs are identified: the majority 24 (89%) because they are within $15''$ of a SCUBA core (criterion **B**)⁵ with the remaining three sources due to their $[3.6] - [4.5]$ and $[8.0] - [24]$ colors (criterion **A**). Table 1 summarizes the sample of candidate embedded YSOs in Ophiuchus. One core, SMM J162626-24243, is associated with two YSOs (GDS J162625.6-242429 and VLA 1623) within $15''$ of its center, although at least one other, SMM J162622-24225, is associated with multiple YSOs (the GSS30-IRS1, -IRS2, -IRS3 system) where only one is picked up as a separate MIPS $24\ \mu\text{m}$ source. This is similar to the analysis from Perseus where only few SCUBA cores were found to be associated with multiple MIPS sources (Jørgensen et al. 2007). It is here worth emphasizing that the resolution of the MIPS observations is only about $6''$ (750 AU) and these numbers should therefore not be taken as statements concerning the close binarity of the embedded YSOs.

Of the 27 embedded YSOs, 16 were also identified as YSO candidates using the criteria used by c2d to extract YSOs based on their mid-infrared colors (see discussion in Harvey et al. 2007), but the remaining 11 were not. This illustrates the need for the combination of mid-infrared and submillimeter data when constructing samples of deeply em-

⁴The selection according to the second criterion “**B**” of course still relies on the association between SCUBA cores and MIPS sources.

⁵Note, that we use the same angular scale for the comparison between the SCUBA cores and MIPS sources in both Ophiuchus and Perseus despite the factor 2 difference in distance between the two clouds. We return to this discussion in Sect. 3.3.

bedded protostars - as it was also concluded based on the analysis of the Perseus data (Jørgensen et al. 2007).

3.2. Distribution of concentrations

An important finding of Jørgensen et al. (2007) was that all cores with concentrations higher than 0.6 had MIPS sources within $15''$. Fig. 6 compares the distributions of the concentrations of the SCUBA cores with and without embedded MIPS sources in Perseus and Ophiuchus. The two distributions are quite different: in Perseus the concentrations of the cores show a very broad distribution with a number of high concentration cores whereas the Ophiuchus distribution shows a pronounced peak at concentrations ≈ 0.35 . In Jørgensen et al. (2007) it was pointed out that protostellar cores should have higher concentrations than pre-stellar, simply because of the heating of the dust from the center. Therefore based on the SCUBA data alone we should expect fewer embedded protostars in Ophiuchus relative to Perseus. This is directly confirmed by comparing the number of SCUBA cores with MIPS sources within $15''$ in the two clouds. Ophiuchus has embedded YSOs in only 23 out of the 66 SCUBA cores while Perseus has embedded YSOs in 42 out of the 72 SCUBA cores. Further, as discussed in §3.4 some of the sources in Ophiuchus are actually disk sources and not deeply embedded.

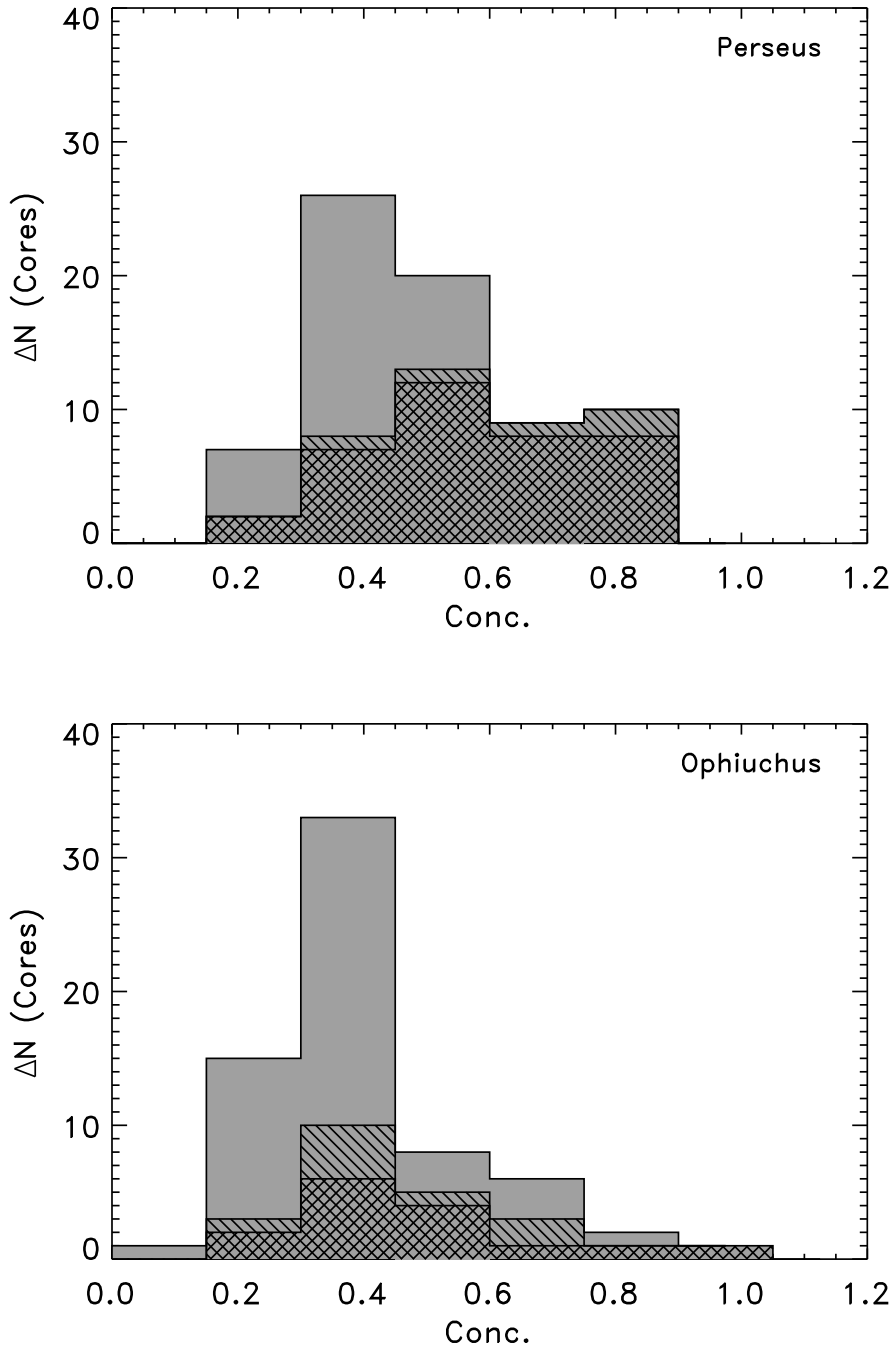


Fig. 6.— Distribution of “concentrations” of SCUBA cores. Those with MIPS sources within 15'' are hatched (single/double) with the cores with MIPS sources with red mid-infrared colors ($[3.6] - [4.5] > 1.0$ and $[8.0] - [24] > 4.5$) within 15'' double-hatched.

3.2.1. Cores with high concentrations and no embedded YSOs

A noteworthy feature of the Ophiuchus SCUBA cores is the existence of four high concentration cores without embedded YSOs. The four cores in Ophiuchus are in fact starless as shown in Fig. 7. Three of these cores are located in the Oph A ridge, which has previously been the subject of detailed studies at (sub)millimeter wavelengths (e.g., André et al. 1993; Wilson et al. 1999). The Spitzer observations confirm that the ridge itself actually appears to be starless but with protostars (e.g., VLA 1623 and GSS 30) located in its immediate vicinity. André et al. (1993) (and likewise Di Francesco et al. (2004)) found that the cores in the Oph A ridge were within a factor two of being in virial equilibrium. Therefore the high concentrations of the cores in the ridge most likely reflect the extreme local pressure due to the surrounding environment. André et al. (1993) found that the millimeter cores in the northern part of the ridge had a high dust temperature of 27 ± 5 K, likely due to heating by the nearby B-star [and clearly heating the dust seen at $24 \mu\text{m}$ also (lower right panel of Fig. 7)].

The fourth high concentration starless core, IRAS 16293E, is a well-studied submillimeter companion to the IRAS source IRAS 16293-2422 and also has no counterparts at $24 \mu\text{m}$ or $70 \mu\text{m}$ (Fig. 7). Castets et al. (2001) suggested that IRAS 16293E was a deeply embedded, or “Class 0” (André et al. 1993), protostar based on the detection of an outflow inferred from HCO^+ . Stark et al. (2004) presented larger scale maps and showed that this was not the case, rather the outflowing motions suggested for IRAS 16293E by Castets et al. were a result of the larger scale outflow driven by IRAS 16293-2422B fanning around IRAS 16293E. The Spitzer images indeed confirm that the IRAS 16293-2422 outflow extends eastwards of IRAS 16293E (Fig. 8). The absence of a central heating source in IRAS 16293E is also consistent with the fact that IRAS 16293E shows strong N_2H^+ emission relative to the protostellar source in IRAS 16293-2422 itself as reported by Castets et al. (2001). N_2H^+ is found to be prominent in starless cores with low temperatures where CO has frozen out on dust grains and thus unavailable to destroy N_2H^+ . In contrast, the conditions within protostellar cores heat a significant part of the envelope to temperatures where CO is released into the gas-phase (e.g., Bergin et al. 2001; Jørgensen et al. 2004). It is likely that the submillimeter core IRAS 16293E is affected by the coincident outflow, e.g., compression and heating possibly increasing its concentration.

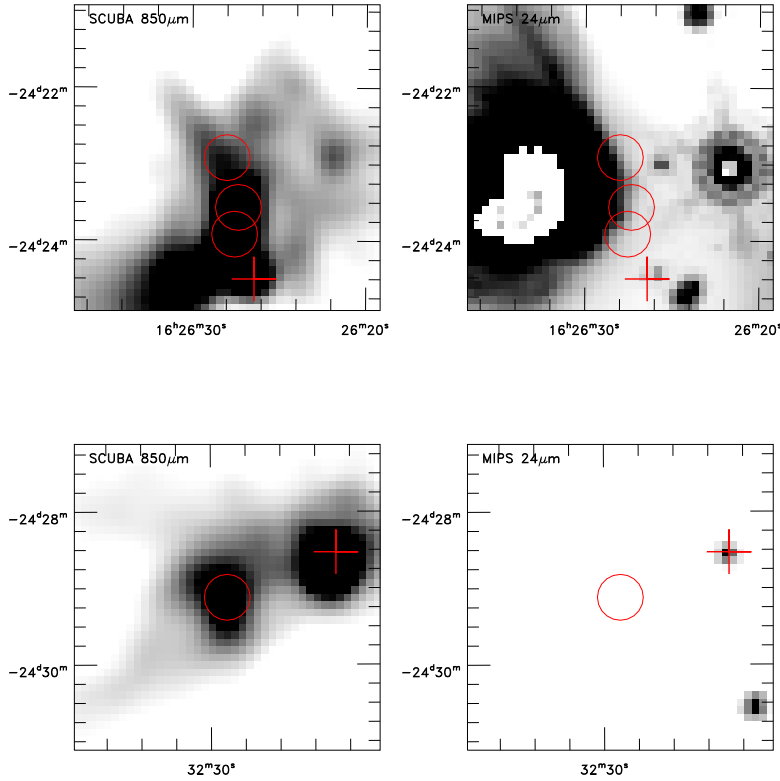


Fig. 7.— Cores with concentrations larger than 0.6 and no embedded YSOs shown on top of the SCUBA $850\ \mu\text{m}$ image (left panels) and the MIPS $24\ \mu\text{m}$ image (right panels). The upper panels show the Oph.-A ridge and the lower panel the region around IRAS 16293-2422. In all panels the circles indicate cores with high concentrations but no associated MIPS sources (SMM J162627-24233, J162628-24225, J16262628-24235 in the upper panels and SMM J163229-24291 in the lower panels) whereas the plus-signs show the location of the known Class 0 sources, VLA 1623 (SMM J162626-24243; upper panels) and IRAS 16293-2422 (SMM J163223-24284; lower panels).

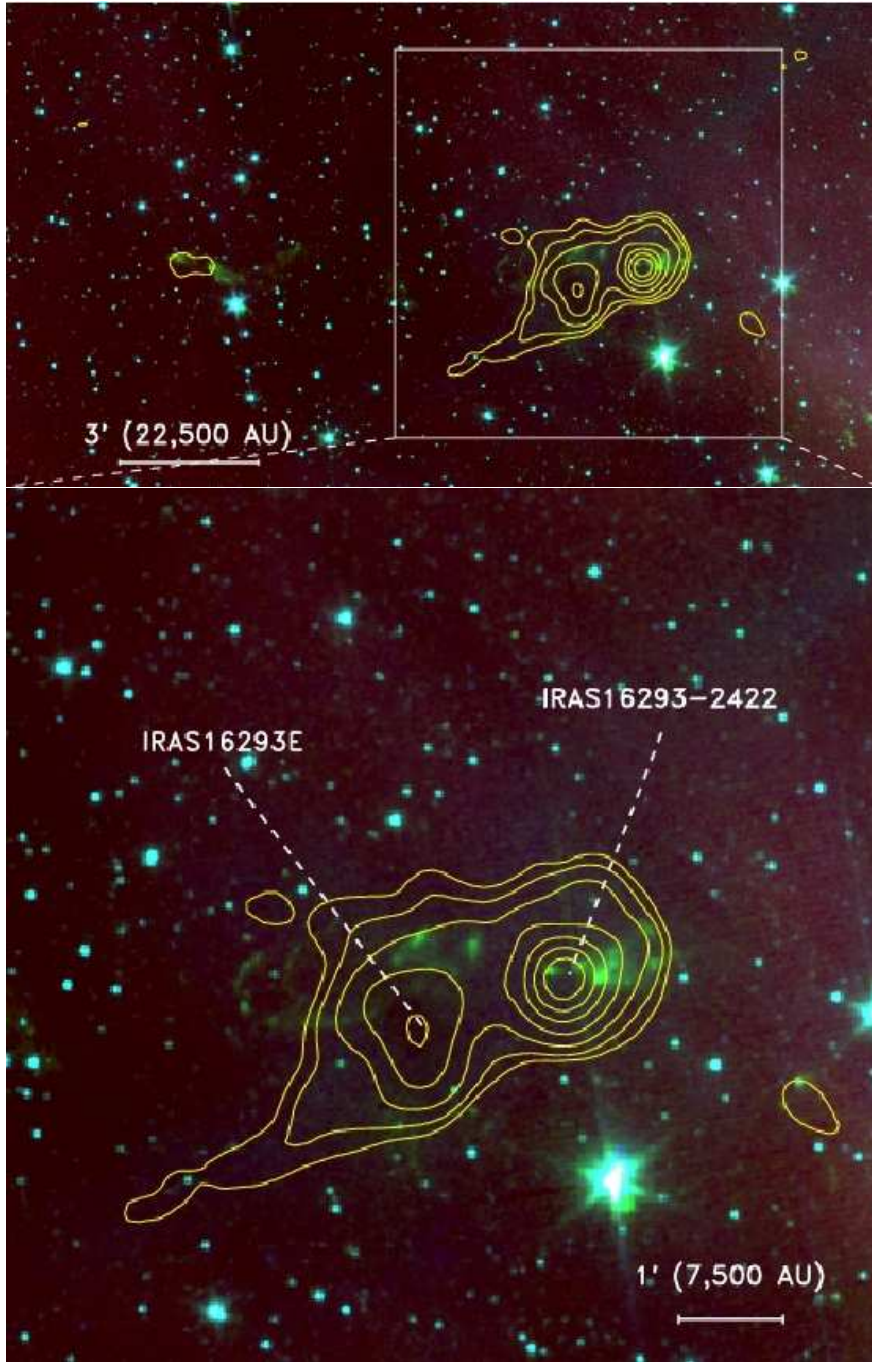


Fig. 8.— Three-color image (blue: IRAC1 $3.6 \mu\text{m}$, green: IRAC2 $4.5 \mu\text{m}$ and red: IRAC4 $8.0 \mu\text{m}$) of the region around the Class 0 protostar IRAS 16293-2422 and starless core IRAS 16293E. The SCUBA map is overlaid in yellow contours. The outflow interaction is predominantly traced by emission from rotational transitions of molecular hydrogen picked up in the IRAC2 band (i.e., the green color; see, e.g., Noriega-Crespo et al. 2004).

3.3. Distance effects

The most obvious limitation in the direct comparison between Perseus and Ophiuchus is the factor of two difference in distance between the two clouds (Perseus at 250 pc; Ophiuchus at 125 pc)⁶. Since the SCUBA and Spitzer surveys are observed to the same absolute depth for each cloud, we would expect intrinsically weaker sources to be detected in Ophiuchus. For example, if we assume that each of the SCUBA cores are isothermal at 15 K the typical 5σ sensitivity of $0.15 \text{ Jy beam}^{-1}$ in the SCUBA maps corresponds to total masses within the $15''$ arcsecond beam (dust+gas) of 0.08 and $0.02 M_{\odot}$ in Perseus and Ophiuchus, respectively.

Since many of the SCUBA cores are barely resolved by only a few beams, resolution might affect the derived physical properties. The factor of two better spatial resolution in Ophiuchus therefore challenges comparisons between the physical properties of the two clouds. Additionally, given the gregarious nature of the submillimeter cores, nearby neighbors will be merged into larger entities in the Perseus cloud. To address both these issues we simulated the case where the SCUBA map of Ophiuchus was observed at the distance of Perseus: the Ophiuchus SCUBA maps were convolved with a beam twice the size of the regular SCUBA beam and the map re-sampled to affect the spatial and pixel resolution of Perseus. Furthermore, the observed brightness was reduced by a factor four, corresponding to the further distance. The Clumpfind algorithm was then applied to this new map to identify substructures. Fig. 9 compares the peak fluxes and concentrations of the SCUBA cores in the original map with the ones in the map simulated at twice the distance.

As expected the number of cores decreases when the cloud is moved to a larger distance: the lower S/N causes the smallest cores to be missed and the larger cores have their sizes reduced, since their boundaries in Clumpfind are defined by the contour at an absolute flux level. Although the total number of cores thereby decreases, the relative distribution of core sizes remains the same as some of the closest cores, e.g., in the Oph A ridge, are merged into larger cores. For the cores with high fluxes the concentration appears to be largely unchanged. For the fainter cores, the cores with the highest concentrations are more likely disappearing as their peaks drop below the detection threshold. The lower concentration faint cores in contrast have a better chance of survival as their faint emission is more evenly distributed and the convolution just moves emission from larger scales into the central beam. Finally, the concentration of the cores formed by a merger of multiple cores tends to be similar

⁶We note that these distance estimates in themselves may contain significant uncertainties: a recent analysis of Hipparcos data for Ophiuchus by Mamajek (2008) for example suggests a consensus distance of 139 ± 6 pc to this cloud whereas distance estimates for Perseus range from about 220 pc to 350 pc (see Enoch et al. (2006) for a discussion).

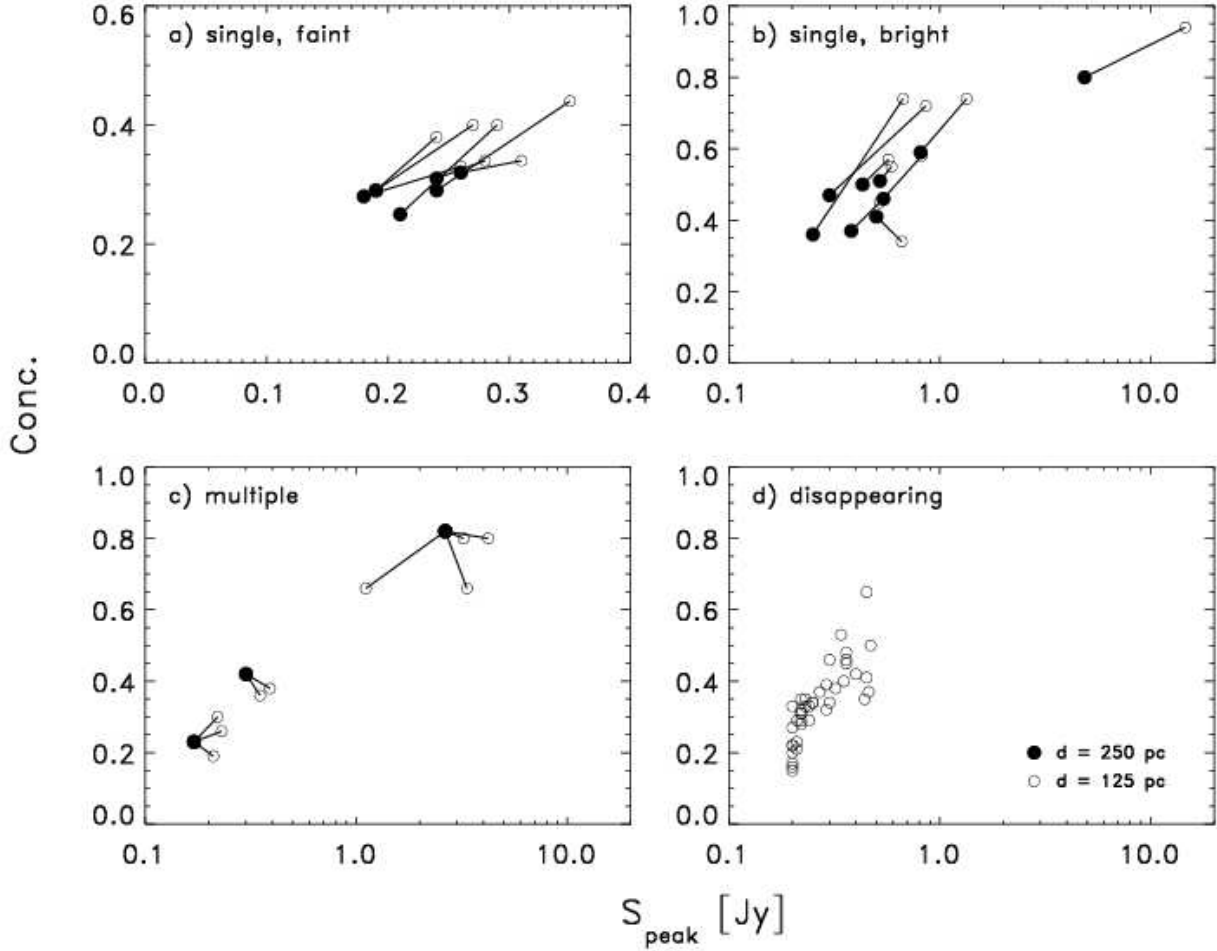


Fig. 9.— Change in peak fluxes and concentrations for the Ophiuchus dataset moved from 125 to 250 pc. In each panel open symbols represent SCUBA cores at 125 pc and closed symbols SCUBA cores at 250 pc. The loss in angular resolution makes individual core identifications ambiguous and thus all cores from the $d = 125$ pc map which lie within one core radius of a measured core at $d = 250$ pc are grouped together. The four panels contain: *a*) single cores in both datasets with peak fluxes smaller than 0.5 Jy, *b*) single cores in both datasets with peak fluxes larger than 0.5 in the original ($d = 125$ pc) dataset, *c*) systems where multiple cores are joined into one core in the more distant cloud and *d*) and cores that fall below the detection limit at the larger distance.

to the highest concentration core merged. Taken together, these effects will bias against low flux, high concentration sources at larger distances, i.e., typically more evolved sources such as embedded objects with lower mass envelopes or disks. The SCUBA maps of Ophiuchus are therefore expected to reveal more sources than Perseus although these will generally be less massive and smaller. This is indeed seen when comparing the list for Perseus (Kirk et al. 2006) with that from Ophiuchus from this paper: the median core radius is 7000 AU (28") in Perseus vs. 3875 AU (31") in Ophiuchus and likewise the median core mass $0.90 M_{\odot}$ in Perseus vs. $0.44 M_{\odot}$ in Ophiuchus.

Since, the criteria for associating a MIPS source with a SCUBA core is based on its distance on angular and not linear scale, a natural question is whether we instead ought to increase the radius from 15" to 30" for associations according to our second criterion, "B". Table 4 summarize the sources separated 15"–30" from a SCUBA core. The numbers in themselves argue that these are not a significant population of embedded YSOs: only 9 MIPS sources are found in this separation range compared to the 24 within 15" of the center of a SCUBA core (the latter covering a factor 3 smaller area). None of these sources have red colors fulfilling our "A" criterion or are associated with well-studied, embedded protostars. On the other hand, it is also not reasonable to decrease the size scale in which SCUBA cores are associated with MIPS sources in Perseus - given the intrinsic uncertainty in the pointing of the submillimeter data (a few arcseconds) and the size of the JCMT/SCUBA beam (15"). That most of the red MIPS sources in fact fall within this radius (e.g., Fig. 4-5) and Jørgensen et al. 2007) suggests that most of scatter seen in this diagram is due to the instrumental limitations and that the distribution in fact is even tighter (typical separations <5-10").

An important, and somewhat subtle, effect is that the distance difference also skews the interpretation of the embedded protostellar sources - compared to the pre-stellar cores. The dust continuum maps measure the optically thin emission from dust, weighted by the temperature within the SCUBA beam. For an optically thin envelope the temperature dependence on radius, r is:

$$T_d(r) = 60 \left(\frac{r}{2 \times 10^{17} \text{ cm}} \right)^{-q} \left(\frac{L_{\text{bol}}}{10^5 L_{\odot}} \right)^{q/2} \quad (1)$$

where $q = 2/(4+\beta)$ depends on the slope of the dust opacity law $\kappa \propto \nu^{\beta}$ (e.g., Chandler & Richer 2000). In more convenient units at a radius corresponding to the 15" size of the SCUBA beam for ISM dust with $\beta = 2$ Eq. 1 becomes:

$$T_d(r) = 21 \left(\frac{d}{125 \text{ pc}} \right)^{-1/3} \left(\frac{L_{\text{bol}}}{1 L_{\odot}} \right)^{1/6} \quad (2)$$

A protostellar envelope will therefore have a dust temperature which increases in the central SCUBA beam as it is brought nearer (25% higher if the distance to the source is halved) and it will brighten significantly (by about 50% at half the distance). This, however, is not the case for the starless cores which are close to isothermal (or actually decreasing in temperature toward their centers) as the actual temperature measured in the SCUBA beam is not varying with radius. We should therefore expect to have an easier task detecting protostellar cores in Ophiuchus relative to Perseus - or correspondingly, be sensitive to even lower masses of envelopes in Ophiuchus relative to Perseus. This will bias the results in a relative sense towards a situation with fewer low-mass protostellar sources compared to pre-stellar cores in the more distant cloud, i.e., Perseus.

The improved sensitivity in the nearer cloud will also cause circumstellar disks to start “contaminating” our sample. Andrews & Williams (2005) surveyed a sample of isolated sources in Taurus with SCUBA, including a number of well-known classical T-Tauri stars, or “Class II” (Lada 1987), YSOs . They found that 35% of those more evolved sources had fluxes larger than 100 mJy (about the 3σ sensitivity limit of our SCUBA maps) whereas less than 10% had fluxes larger than 500 mJy. The distance to Taurus ($d = 140$) and Ophiuchus ($d = 125$) are comparable and thus we would expect to pick up some more evolved, “Class II” young stellar objects without envelopes in the Ophiuchus SCUBA data. In contrast the 10% cut-off from Taurus would be moved to a flux of 125 mJy in Perseus which would be very close to the sensitivity limit of our SCUBA maps.

Table 1: List of candidate embedded YSOs in Ophiuchus.

RA (J2000) ^a hh mm ss.ss	DEC (J2000) ^a dd mm ss.s	Conc. ^b	[3.6] – [4.5]	[8.0] – [24]	Sep. ^c [$''$]	SCUBA flux ^d [Jy beam ⁻¹]	Code ^e	Common identifiers ^f
16 26 10.32	-24 20 54.6	0.65	0.81	2.66	3.4	0.45	-BC	● GSS 26
16 26 14.63	-24 25 07.5	0.34	7.8	0.28	AB-	...
16 26 17.23	-24 23 45.1	0.32	1.20	3.23	3.1	0.29	-B-	● CRBR 12 / ISO-Oph 21
16 26 21.35	-24 23 04.3	0.58	1.31	...	10.2	0.82	AB-	● Elias 21 / GSS 30-IRS1 ^g
16 26 24.07	-24 16 13.4	0.41	0.54	2.30	2.5	0.45	-B-	BKLT J162624-241616 / Elias 24
16 26 25.46	-24 23 01.3	0.66	1.06	5.33	35.2	0.34	A-	● CRBR 2324.1-1619 / [GY92] 30
16 26 25.62	-24 24 28.9	0.80	2.12	6.77	11.5	3.23	ABC	GDS J162625.6-242429
16 26 26.42	-24 24 30.0	0.80	1.0	3.23	ABC	● VLA 1623
16 26 40.46	-24 27 14.3	0.53	0.91	4.07	1.9	0.34	-B-	● BKLT J162640-242715 / [GY92] 91
16 26 44.19	-24 34 48.4	0.29	1.72	...	3.2	0.24	AB-	● WL 12 / ISO-Oph 65
16 26 45.02	-24 23 07.6	0.74	0.76	2.68	3.1	0.67	-BC	● BKLT J162645-242309 / Elias 27 / GSS 39 / VSSG 28
16 26 58.42	-24 45 31.8	0.42	0.52	2.53	6.6	0.40	-B-	SR 24N / Elias 28
16 26 59.10	-24 35 03.3	0.55	1.2	4.9	38.6	0.17	A-	● WL 22 / ISO-Oph 90
16 27 05.24	-24 36 29.6	0.34	1.09	5.36	1.6	0.25	AB-	● CRBR 2403.7-2948 / [GY92] 197
16 27 06.75	-24 38 14.8	0.22	1.08	3.89	4.6	0.20	-B-	CRBR 2404.8-3133 / WL 17
16 27 09.40	-24 37 18.6	0.48	1.4	0.36	AB-	● Elias 29 / WL 15 / CRBR 2407.8-3033
16 27 26.91	-24 40 50.7	0.57	1.22	...	3.8	0.57	AB-	● YLW15 / IRS43 / IR16244-2434
16 27 27.99	-24 39 33.4	0.37	1.48	...	1.0	0.27	AB-	● YLW16 / IRS44 / IR16244-2432
16 27 28.44	-24 27 21.0	0.34	0.89	2.81	12.5	0.66	-B-	[AMD2002] J162728-242721
16 27 30.17	-24 27 43.2	0.50	1.00	2.20	9.7	0.47	-B-	● Elias 33 / VSSG 17
16 27 39.81	-24 43 15.0	0.27	0.70	3.40	1.9	0.20	-B-	● IRS51 / IR16246-2436
16 28 21.61	-24 36 23.4	0.39	2.08	6.03	2.8	0.29	AB-	(●) [SSG2006] MMS126 / IR16253-2429
16 31 35.65	-24 01 29.3	0.72	1.01	3.25	2.6	0.86	-BC	GWAYL 4 / IR16285-2355
16 31 52.45	-24 55 36.2	0.40	1.21	4.59	30.5	0.12	A-	ISO-Oph 203
16 32 00.99	-24 56 42.6	0.45	1.46	...	1.4	0.36	AB-	[B96] L1689S1 3 / ISO-Oph 209
16 32 22.63	-24 28 31.8	0.94	6.5	14.6	ABC	IR16293-2422
16 33 55.60	-24 42 05.0	0.33	0.15	4.49	1.7	0.20	-B-	RX J1633.9-2442

^aPosition of Spitzer source from c2d catalog.

^bConcentration of the nearest SCUBA core.

^cSeparation between the Spitzer source and SCUBA core.

^dFor sources with code “A–” the SCUBA flux refers to flux density at the exact position in the maps; for the remaining sources to the peak flux from the Clumpfind algorithm.

^eIdentifier indicating whether the given source obeys (**A**: MIPS 24 μ m source with $[3.6] - [4.5] > 1$ and $[8.0] - [24] > 4.5$, **B**: separation between Spitzer source and nearest SCUBA core less than $15''$ and **C**: Associated submillimeter core has concentration higher than 0.6). Note only **A** and **B** are used to construct this sample.

^fist of common identifiers from the SIMBAD database (IR=IRAS). Sources indicated with “●” are included in the list of embedded YSOs by Wilking et al. (2008).

^gA complex system of at least three protostellar candidates: in addition to GSS30-IRS1 a nearby source is seen at 16:26:22.38; -24:22:52.9 at a distance of $10.4''$ from the SCUBA core: [AMD2002] J162622-242254 / VSSG 12 / ISO-Oph 34 / GSS 30-IRS2. A third source, ● GSS 30-IRS3 / LFAM 1, is at 16:26:21.72 -24:22:50.5, separated by $4.5''$ and with $[3.6] - [4.5] = 0.9$ and $[8.0] - [24] = 5.3$ (although with low S/N in MIPS1 due to confusion with GSS30-IRS1).

Table 2: As Table 1 for SCUBA cores in Ophiuchus with high concentrations and no embedded YSOs (see also Table 7).

Name (SMM J)	RA (J2000)	DEC (J2000)	Conc.	Sep.	SCUBA flux	Common identifiers
162627-24233	16 26 27.34	-24 23 33.9	0.66	19.6	3.350	
162628-24235	16 26 27.55	-24 23 54.9	0.80	25.8	4.220	
162628-24225	16 26 28.00	-24 22 54.9	0.66	35.2	1.110	[MAN98] A-MM6
163229-24291	16 32 29.06	-24 29 07.2	0.74	94.7	1.340	IRAS 16293E

Table 3: As Table 1 for interesting MIPS sources with very red colors, but no associated SCUBA flux (e.g., candidate edge-on disks)..

RA (J2000)	DEC (J2000)	Conc.	[3.6] – [4.5]	[8.0]-[24]	Sep.	SCUBA flux	Code	Common identifiers
16 21 45.13	-23 42 31.6	0.34	1.03	5.25	4256.5	0.033	A–	...
16 21 59.55	-23 16 02.5	0.41	1.11	4.86	5122.8	0.007	A–	...
16 27 38.93	-24 40 20.5	0.31	1.05	4.73	136.8	0.007	A–	BKLT J162738-244019
16 27 48.23	-24 42 25.4	0.27	1.14	5.17	123.5	0.005	A–	...
16 31 52.06	-24 57 26.0	0.46	1.22	4.69	69.3	-0.026	A–	ISO-Oph 202
16 31 56.87	-24 54 03.2	0.40	1.36	4.50	124.2	-0.026	A–	...

Table 4: As Table 1 for sources with separations of 15''-30'' of a MIPS source..

RA (J2000)	DEC (J2000)	Conc.	[3.6] – [4.5]	[8.0]-[24]	Sep.	SCUBA flux	Code	Common identifiers
16 26 25.99	-24 23 40.5	0.66	1.86	2.47	19.6	0.57	...	
16 27 10.02	-24 29 13.1	0.21	0.43	4.97	24.5	0.12	[GY92] 218	
16 27 11.82	-24 39 47.6	0.29	26.1	0.11	...	
16 27 15.50	-24 30 53.6	0.34	1.03	2.81	30.0	0.29	[GY92] 238	
16 27 30.91	-24 27 33.2	0.50	1.64	3.04	20.7	0.38	• [AMD2002] J162730-242734 / ISO-Oph 150	
16 27 37.23	-24 42 37.9	0.31	0.96	3.62	21.0	0.12	[GY92] 301	
16 27 37.88	-24 42 10.8	0.31	1.21	...	29.1	0.04	...	
16 27 41.02	-24 43 32.4	0.27	24.7	0.02	...	
16 31 33.52	-24 3 34.5	0.35	0.14	1.38	23.2	0.12	...	
16 31 34.29	-24 3 25.2	0.35	0.73	2.58	26.0	0.14	...	
16 31 52.11	-24 56 15.8	0.40	0.90	2.95	28.1	0.20	L1689-IRS5	

3.4. Comparison to other mid-infrared and submillimeter surveys

While the Spitzer observations of Ophiuchus are unprecedented at mid-infrared wavelengths in terms of the area covered and sensitivity, a number of surveys have covered similar areas of the cloud at (sub)millimeter wavelengths. Besides JCMT/SCUBA observations (Johnstone et al. 2000a; Visser et al. 2002; Johnstone et al. 2004; Nutter et al. 2006), Ophiuchus has been surveyed at 1.1–1.2 mm using the MAMBO bolometer on the IRAM 30 m telescope (Motte et al. 1998), the SIMBA bolometer on the SEST telescope (Stanke et al. 2006) and Bolocam on the Caltech Submillimeter Observatory 10.4 meter telescope (Young et al. 2006).

Our number of cores, 66, is somewhat lower than the 100 submillimeter cores originally reported by Johnstone et al. (2004): Johnstone et al. went down to a much deeper depth ($0.02 \text{ Jy beam}^{-1}$) than we have done here mainly to confirm that their main result (the absence of cores at low A_V) was not a result of a biased look at only the brightest cores. We do not include these fainter sources here for consistency with the Kirk et al. (2006) and Jørgensen et al. (2007) studies of Perseus.

Nutter et al. (2006) surveyed L1689B in the submillimeter, using a subset of the SCUBA 850 μm data presented here. By going to a lower noise level, they identified about twice as many dust continuum cores compared with the list used in this paper. These “extra” cores are predominantly fainter emission stretching over arcminute scales. For the brighter, more concentrated cores, there is a direct one-to-one mapping between our sample and that of Nutter et al.. Likewise none of the “extra” cores in the list of Nutter et al. have associated MIPS sources within $30''$ - consistent with their starless nature as also found by Nutter et al..

Wilking et al. (2008) listed a sample of 35 embedded YSOs in L1688 based on near- and mid-infrared surveys, in particular, the ISO survey of Ophiuchus by Bontemps et al. (2001). Of these sources 15 (16 if one includes LFAM 1 which is a faint companion to GSS30-IRS1 in our list; see footnote to Table 1) are common with our list (22 of the objects from our list associated with L1688). Wilking et al. also mentions [SSG2006] MMS126 as a potential Class 0 source, although it is not included in their list. The list also includes sources that are associated with well-studied YSOs, including IRS 46 (Lahuis et al. 2006) and IRS 48 (Geers et al. 2007) that both show little submillimeter emission and have been suggested to be disk sources. Two sources from the list are associated with regions of strong submillimeter emission but are likely also disk candidates: one is CRBR 2422.8-3423 modeled in detail by Pontoppidan et al. (2005) who suggested that it was a disk seen edge-on. It is not associated with a separate peak in the SCUBA map (the emission being dominated by the nearby protostar, YLW 15 or IRS 43) although with a flux of $0.39 \text{ Jy beam}^{-1}$ at the location of the MIPS source and colors, $[3.6] - [4.5] = 1.4$ and $[8.0] - [24] = 4.45$, it just misses

the criteria in this paper. ISO-Oph 150 (IRAC 30 in the list of Wilking et al. (2008)) shows similar red $[3.6] - [4.5]$ colors and likewise has a SCUBA flux of $0.37 \text{ Jy beam}^{-1}$, but even bluer $[8.0] - [24]$ colors than CRBR 2422.8-3423. It is possible that similar sources are present in our list, but the only way to systematically filter such sources would be either high angular resolution observations (at mid-infrared or submillimeter wavelengths) - or spectroscopical confirmation. Table 3 lists the most prominent candidates edge-on disk sources with no associated SCUBA emission. The remaining sources in the Wilking et al. (2008) are found to show little if any submillimeter emission and/or $[3.6] - [4.5]$ and $[8.0] - [24]$ colors that do not full-fill our criteria, but are bluer. This would suggest that these sources are either only slightly embedded or perhaps more evolved sources extinguished by a large amount of foreground material.

Two of the sources in our list, but which are not included in the list of Wilking et al. (2008), BKL T J162624-241616/Elias 24 and SR 24N/Elias 28, are optically visible and have optically-determined spectral types (e.g Wilking et al. 2005; Struve & Rudkjøbing 1949). These sources do not show particularly red mid-IR colors but are located within a few arcseconds of the center of SCUBA cores, SMM J162624-24162 and SMM J162659-24454, respectively. Both of these SCUBA cores have effective radii less than $15''$ and masses less than $0.1 M_{\odot}$. This suggests that these sources only have tenuous envelopes and that the dust continuum emission largely has its origin in their circumstellar disks.

One source in L1689 selected based on our criteria, SSTc2d J163355.6-244204, is likely also a more evolved object. It is associated with an X-ray source, RX J1633.9-2422, and although it is located only $1.7''$ from the center of a faint SCUBA core (0.2 Jy), its colors do not obey the criteria for embeddedness. The SCUBA core also appears unresolved, consistent with it being submillimeter emission from a compact disk. This illustrates that the “ABC classification scheme” should be taken as a gradation of the likely embeddedness of a given source: the more criteria passed for a given source, the greater likelihood that source is embedded.

3.5. Extended cloud emission and absorption of mid-IR emission

As discussed by Padgett et al. (2008), the MIPS 24 μm images of Ophiuchus show large swatches of variable brightness extended emission across the cloud. In particular, Padgett et al. draw attention to significant dark patches where up to 80% of the extended background emission is absorbed (their Fig. 4). Recently Stutz et al. (2007) analyzed Spitzer images of a similar shadow of the Bok Globule CB 190.

Fig. 10 compare the 24 μm images to SCUBA continuum maps for four cores seen across the field. The resemblance between the shape of the core absorption shadows at 24 μm and their emission profiles at 850 μm illustrate (1) the good correspondence between the resolution at these two wavelengths (6'' at 24 μm and 15'' at 850 μm) and (2) that these cores contain very dense material. A decrease in flux by 80% corresponds to an optical depth of the 24 μm shadow of 1.6 or a visual extinction $A_V = 35$ under the same assumptions as Stutz et al. and assuming that the cores are in the foreground to the extended emission. In reality both zodiacal light and foreground emission (i.e., emission from cloud material in which the core is embedded) may contribute to the observed profile - and the derived extinction is therefore a lower limit to the actual extinction toward the core profiles. For comparison, for a temperature of 10 K the typical SCUBA peak 850 μm fluxes of these cores of 0.2–0.8 Jy beam⁻¹ correspond to an extinction of $A_V = 30 - 70$ averaged over the 15'' SCUBA beam.

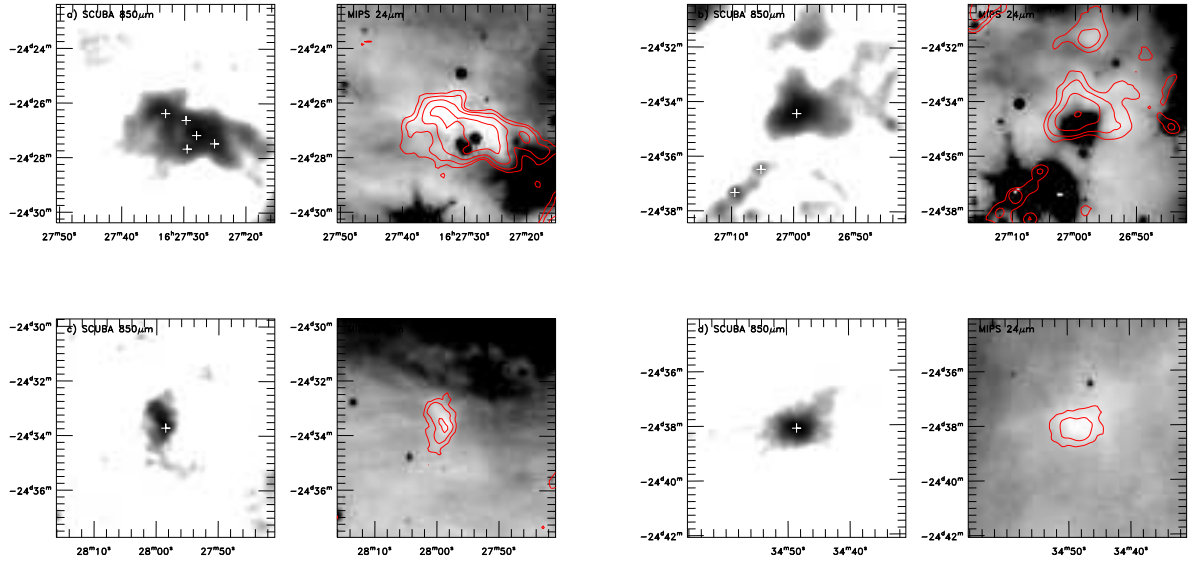


Fig. 10.— 24 μm shadowed cores in the SCUBA 850 μm maps (left) and MIPS 24 μm maps (right). In both panels dark is high intensity of the emission and white is low intensity. The contours in the righthand panels indicate the SCUBA 850 μm emission. The location of the identified SCUBA cores (Table 7) are indicated by white plus-signs in the righthand panels: in *a*) SMM J162725-24273, J162728-24271, J162729-24274, J162730-24264, J162733-24262, *b*) SMM J162660-24343, J162705-24363, J162709-24372, *c*) SMM J162759-24334 and *d*) SMM J163448-24381.

4. Characterizing the current star formation populations

4.1. Motions of YSOs and dissipation of cores

As discussed by, e.g., Harvey et al. (2007), the Spitzer data provides large samples of YSOs that can be classified in the traditional scheme for the evolution based on their spectral indices at near- and mid-infrared wavelengths, α ⁷. This scheme does not directly capture differences within the group of embedded sources which are typically classified into “Class 0” and “Class I” according to their submillimeter signatures (see discussion in § 5.3), e.g., their submillimeter relative to total luminosities. Such a distinction therefore requires fully sampled SEDs as presented, e.g., by Hatchell et al. (2007) and Enoch et al. (2008). Still, since we expect almost all Class 0 sources to be detected at 24 μm and these sources per definition are associated with submillimeter cores, our sample of embedded YSOs is expected to be complete with respect to these sources. For the remainder of this section we therefore use the term “Class I” in the sense of the α -classification scheme which thereby also encompass the more deeply embedded sources.

The distribution of the more evolved YSOs identified by the Spitzer data (e.g., “Flat spectrum”, Class II) compared to the SCUBA cores provides insight into the dynamical properties of star formation. Table 5 lists the number of YSOs in each Class for both Perseus and Ophiuchus from the classification given in the catalogs from the final delivery of c2d data (Evans et al. 2007) and gives the fraction which are located within 15” and 30” of a SCUBA core relative to the total number of YSOs within the area covered by SCUBA. The fraction of embedded YSOs associated with submillimeter cores are clearly decreasing from more than half to less than a few percent in the Class II stages. The numbers suggest both that Class II sources are genuine envelope-less sources and that about 40–50% of the Class I sources do not have envelopes more massive than the sensitivity limit of the SCUBA survey, i.e., about $0.1 M_{\odot}$. This is further illustrated in Fig. 11, which shows the [3.6] – [4.5] vs. [8.0] – [24] color-color diagrams for Ophiuchus and Perseus. In both diagrams the evolved YSO population based on their α (“Flat spectrum”, Class II and Class III) has been separated from the Class I sources. The latter group has furthermore been divided into Class I sources that are or are not within 15” from the center of a SCUBA core. Fig. 11 shows that the Class I sources in Perseus that are not associated with a SCUBA core are located close to the more evolved population of YSOs in this diagram, i.e., typically have less red colors than those that do lie within 15” of a core. This again suggests that these sources are more evolved

⁷The spectral index, α , where $\nu F_{\nu} \propto \nu^{\alpha}$ is calculated in the c2d catalogs from a least square fit to the observations from 2.2 to 24 μm . Following Greene et al. (1994), Class I sources have $\alpha > 0.3$, “Flat Spectrum” sources $-0.3 < \alpha \leq 0.3$ and Class II sources $-1.6 < \alpha \leq -0.3$.

and although they may be associated with envelopes providing their increasing SEDs in the mid-infrared, those envelopes have masses smaller than the sensitivity limit of the SCUBA survey. On the other hand, the population of red sources associated with SCUBA cores seen prominently in the Perseus panel is absent in the Ophiuchus panel, arguing in favor of the more evolved/less embedded nature of the Class I sources in Ophiuchus.

Naturally per definition most (89%) of the sources in the sample constructed in this paper (Table 1) are associated with SCUBA cores with the few exceptions being red sources in region of crowded submillimeter emission. This sample is expected to contain both Class 0 and I protostellar sources.

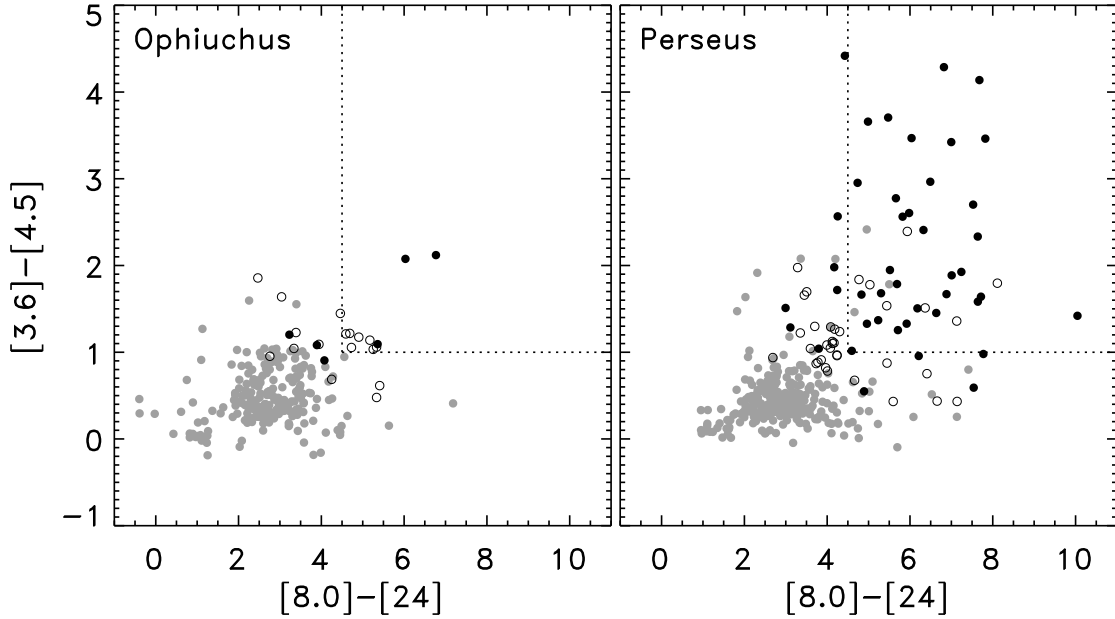


Fig. 11.— $[3.6] - [4.5]$ vs. $[8.0] - [24]$ color-color diagram for the YSOs identified by the c2d color criteria. The “evolved” YSOs (“Flat spectrum”, Class II and Class III) have been shown with grey symbols whereas the Class I YSOs are shown with black symbols. The Class I YSOs have furthermore been divided into those that are (filled symbols) and are not (open symbols) located within $15''$ of a SCUBA core. The dotted lines indicate the color criteria for embedded YSOs ($[3.6] - [4.5] > 1.0$ and $[8.0] - [24] > 4.5$). The Class I sources that are not associated with SCUBA cores are found close to the more evolved YSOs in this diagram, suggesting that these sources are less embedded and have envelopes with masses below the detection limit of the SCUBA survey ($0.1 M_{\odot}$).

Table 5: Number of mid-infrared classified YSOs within 15'' or 30'' within SCUBA cores and in total.

Class	Ophiuchus (265 total)			Perseus (353 total)		
	Within 15''	Within 30''	Total	Within 15''	Within 30''	Total
I	15 (47%)	17 (53%)	32	49 (58%)	55 (66%)	84
Flat spectrum	4 (9.1%)	8 (18%)	44	4 (9.5%)	6 (14%)	42
II	5 (3.1%)	5 (3.1%)	163	2 (1.0%)	6 (3.0%)	199
III	0 (0.0%)	0 (0.0%)	26	0 (0.0%)	1 (3.6%)	28
<i>This paper</i> ^a	24 (89%)	24 (89%)	27	50 (94%)	51 (96%)	53

^aSamples of embedded objects from this analysis.

The decrease in fraction of sources associated with submillimeter cores in the later YSO classes can be interpreted in two ways: either the envelopes around the embedded sources dissipate over the duration of the Class I stage or the YSOs themselves disperse (i.e., move away from their parental cores through their evolution). However, although the number of red YSOs in Ophiuchus is lower than in Perseus these are still strongly clustered within $15''$ (§3.1 and Fig. 3). As discussed in Jørgensen et al. (2006) this in itself suggests that very little dispersal of the YSOs take place during their evolution through their embedded stages. In fact, this is likely to be expected given the required escape velocity from centers of the SCUBA cores: the median mass of $M_0 = 0.44 M_\odot$ and radius of $r_0 = 31''$ (3875 AU) of the cores from Table 7 corresponds to an escape speed from the center of a constant density core to infinity, $v = \sqrt{3GM/r_0}$, of 0.5 km s^{-1} - about 5 times the sound speed in a molecular cloud with a temperature of 10–15 K. As the density profile of the SCUBA cores are centrally condensed (and the escape velocity thus higher) it therefore shows that highly supersonic motions would be required at the birth of the central protostar in order for it to escape its parental core during the embedded protostellar stages.

4.2. Nearest neighbor surface and volume density maps

As discussed in Jørgensen et al. (2006) and Padgett et al. (2008), on large scales the Perseus and Ophiuchus clouds are highly non-uniform. Significant star formation occurs in well-defined regions, e.g., the two main clusters, IC 348 and NGC 1333, of Perseus or L1688 in Ophiuchus. On the other hand significant star formation was also found to occur outside of these clusters in Perseus, e.g., in the smaller groups surrounding B1, L1448 and L1455. Fig. 12 compares the distribution of red MIPS sources around the cores in NGC 1333, IC 348 and the rest of the cloud (using the distinction between the two clusters and the remainder of Perseus from Jørgensen et al. (2006)). As seen in this figure the “extended” region which predominantly covers SCUBA cores in the smaller groups, B1, L1448 and L1455, shows the most concentrated distribution of YSOs around the center of the SCUBA cores whereas IC 348 in the other extreme shows the most loose distribution of YSOs. This in itself suggests that the smaller groups are still in the early star forming stages, whereas the region around IC 348 predominantly contains more evolved YSOs that are no longer associated with SCUBA cores.

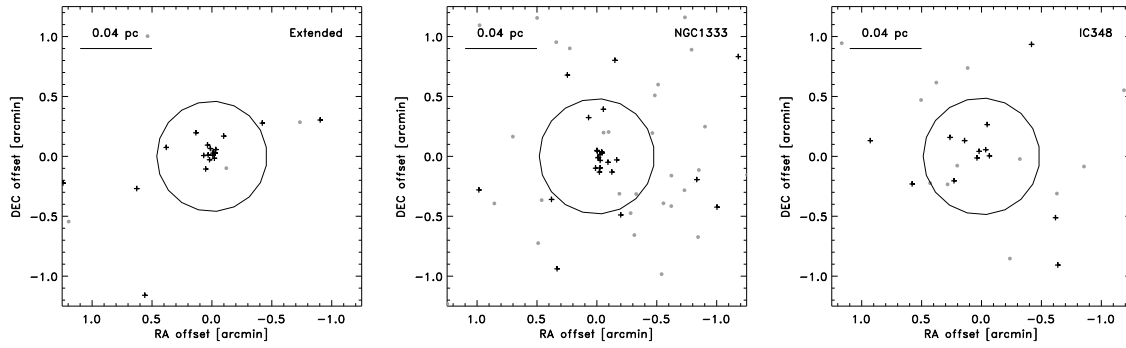


Fig. 12.— As Fig. 3 showing the distribution of MIPS sources around each SCUBA core (shifted to the same center) for subregions in Perseus: the extended cloud, NGC 1333 and IC 348. The concentration of red MIPS sources (black plus signs) are seen to be significantly higher in the two former regions than in IC 348 suggesting differences in their star formation histories.

Many quantifiable properties about individual star-forming regions depend on the choice of boundary used to describe the region. For example, the star formation efficiency depends on the gas mass enclosed within a given region surrounding YSOs. It is thus important to have objective criteria for defining the boundaries of subregions within clouds and determining the memberships of these groups. To apply this in a systematic fashion we utilize a nearest-neighbor algorithm similar to that discussed by Gutermuth et al. (2005) (see also Casertano & Hut 1985). Across the cloud we calculate the local surface density, σ , at grid position (i, j) from

$$\sigma = \frac{n - 1}{\pi r_n^2(i, j)} \quad (3)$$

where $r_n(i, j)$ is the distance to the n 'th nearest neighbor (following Gutermuth et al., $n = 5$). Assuming local spherical symmetry the volume density, ρ , can likewise be defined as:

$$\rho = \frac{n - 1}{\frac{4}{3}\pi r_n^3(i, j)} \quad (4)$$

From Eq. 3 and 4 it is easily seen that $\rho = \frac{3}{4}\sqrt{\frac{\pi}{n-1}}\sigma^{3/2}$ under these assumptions. In case the distribution of sources are flattened along the line of sight, the derived volume density is a lower limit to the actual volume density.

As discussed by Gutermuth et al. and others this is just one of the many different ways to quantify the substructure of clouds and we do not attempt to address fundamental questions such as what fraction of stars form in isolation and clusters and whether the star formation process is hierarchical or fractal in nature. We also note that significant substructure exists within the regions defined in this manner (see, e.g., study of NGC 1333 by Gutermuth et al.). A more exhaustive analysis of the clustering substructure in these clouds is outside the scope of this work.

As input for this analysis we use the list of YSO candidates from the catalogs included in the final delivery of c2d data (Evans et al. 2007). These lists of YSOs include sources identified using their mid-infrared colors (e.g., Harvey et al. 2007) as well as the deeply embedded protostars from this work. These lists are therefore restricted to YSOs with a mid-infrared excess, i.e., predominantly YSOs the Class 0–II evolutionary stages. The results of this analysis is shown in Fig. 13 for Ophiuchus and Perseus.

Lada & Lada (2003; LL03 in the following) compiled a catalog of clusters, defining those as being groups of stars stable against tidal disruption by the galaxy or passing interstellar clouds. This criterion translates to a mass density of $1.0 M_\odot \text{ pc}^{-3}$ (or 2 sources pc^{-3} for an IMF with a mean mass of $0.5 M_\odot$ or a surface density of $2.1 \text{ sources pc}^{-2}$ with the

assumption of local spherical symmetry). In addition, LL03 required clusters to have more than 35 members to ensure that its evaporation time was larger than 10^8 years. The volume density level of LL03 is shown in both panels of Fig. 13 with the blue contour while the black contours correspond to volume densities 0.125, 0.25, 0.5, 2, 4 and 8 times this level. It is clear that the volume density contour suggested by the stability arguments of LL03 does not capture the substructure of the YSO distributions, but rather that a higher contour level is required. A similar issue is seen when applying the algorithm to the samples of in Serpens (Harvey et al. 2007): there a much higher surface density encompasses the entire surveyed region. It thus appears that the LL03 criterion is too loose to capture the substructure of the regions. This becomes even more aggravated by the fact that our YSO catalogs do not include the most evolved YSOs, those with little mid-infrared excesses. If these were included in the lists of YSOs, the groups would be found to cover even larger areas and volumes. Judging by eye, a volume density twenty-five times higher than the LL03 level (yellow contour in Fig. 13) appears to better capture the structure of the YSO distributions seen in these clouds.

We thus use the following criteria to determine the subgroupings of YSOs (“associations”) within the c2d clouds: we define associations of YSOs as loose or tight depending on whether they have a minimum volume density of $1 M_{\odot} \text{ pc}^{-3}$ ($1 \times \text{LL03}$) or $25 M_{\odot} \text{ pc}^{-3}$ ($25 \times \text{LL03}$). The associations are furthermore split into “clusters” (greater than 35 members) and “groups” (less than 35 members). Due to the definition of surface/volume density from the fifth nearest neighbor, the lower limit to the number of members in a given group is 5.

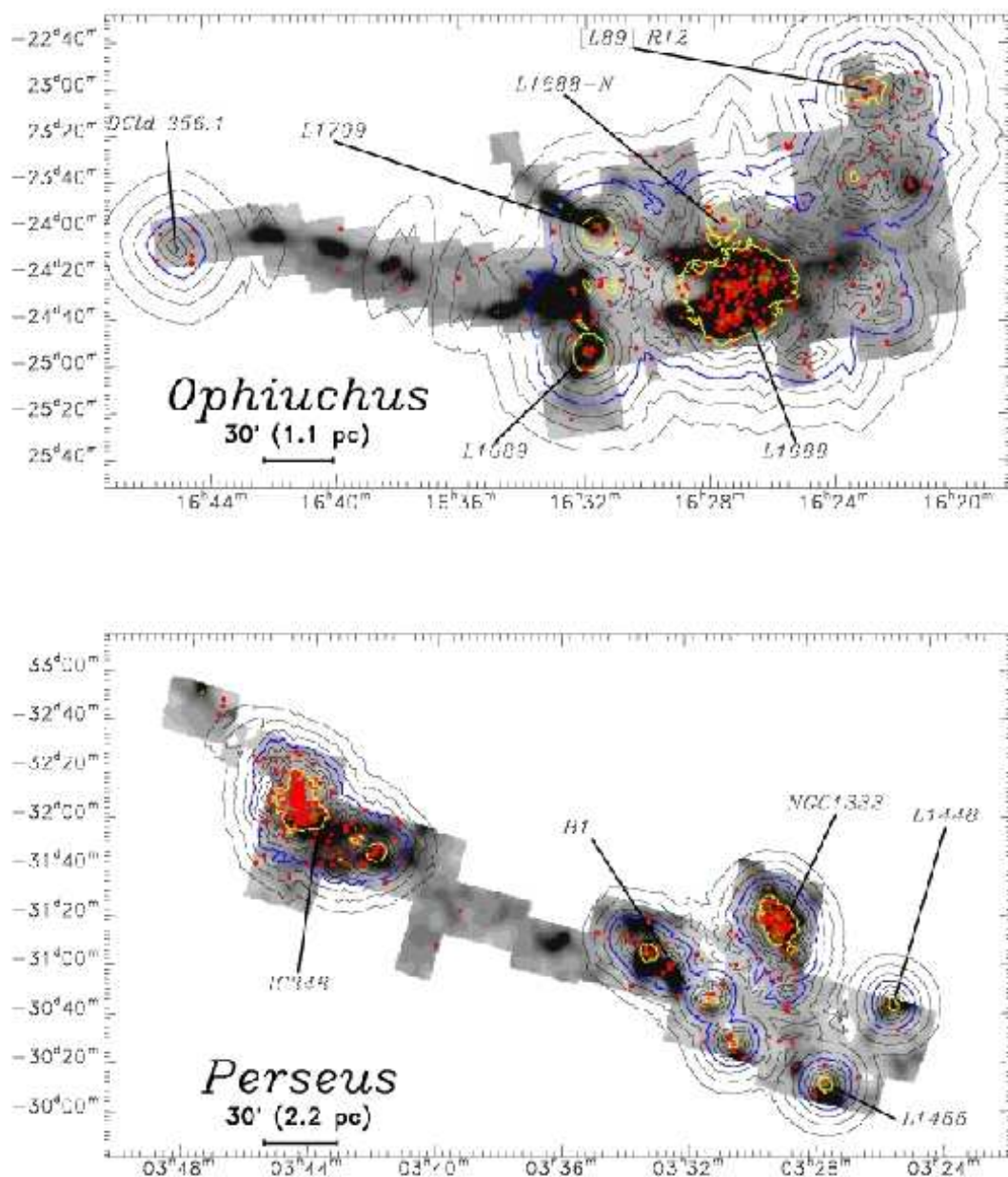


Fig. 13.— Volume density contours of the YSOs in Ophiuchus (upper panel), Perseus (lower panel) shown on top of extinction maps (grey-scale) based on the c2d data (Evans et al. 2007). In both panels the black contours indicate the volume densities corresponding to 0.125, 0.25, 0.50, 2.0 and 4.0 $M_{\odot} \text{pc}^{-3}$. The blue contours show volume densities of 1 $M_{\odot} \text{pc}^{-3}$, corresponding to the criterion ($1 \times \text{LL03}$ in the text) for identifying clusters suggested by Lada & Lada (2003), and the yellow contours to volume densities of 25 $M_{\odot} \text{pc}^{-3}$ ($25 \times \text{LL03}$ in the text). The red dots show the locations of the YSOs and the green plus signs the locations of the SCUBA cores in the two clouds.

4.2.1. Substructure of Ophiuchus

At the $1 \times \text{LL03}$ level most of the YSOs in Ophiuchus are included in one large region, “e-Oph”, encompassing the main associations of YSOs around L1688, L1709 and L1689. The only other loose group is located close to DClD 356.1+13.7 (Feitzinger & Stuewe 1984) in the northwestern part of the Ophiuchus streamer. This loose group is located slightly to the south of a ^{13}CO core, [L89] R76, in the maps of Loren (1989). This region was not covered by the SCUBA maps (although inside the c2d coverage - and thus the extinction maps in Fig. 13). The same is true for the two extinction cores associated with L1712 and L1729 [seen in the c2d maps at (16:40;-24:10) and (16:42;-24:10)] which do not contain any YSOs.

At the higher $25 \times \text{LL03}$ level, the main loose cluster, “e-Oph”, is broken into five separate tight regions. The dominating tight concentration is associated with the L1688 dark cloud which contains 171 members (61% of those in the larger loose cluster) and is the only “cluster” in Ophiuchus according to our definition. It also dominates in terms of the number of SCUBA cores, with 71% of the SCUBA cores (83% of those associated with MIPS sources).

Four additional tight regions have 5–10 members each and are therefore classified as “groups”. Only two of these regions have SCUBA cores within their boundaries; those associated with the dark clouds L1689 and L1709. L1689 and L1709 show extended dust extinction but only small regions containing embedded YSOs. In L1709 a small group of starless cores are identified at the DCO^+ peak, L1709A, from the maps of Loren et al. (1990) (see also Fig. 2). The small group of YSOs at the peak of the L1709 filament is associated with the IRAS point source, IRAS 16285-2355. In L1689 the YSO density peaks at the southern part of the extinction core associated with L1689S (Loren 1989). A few additional isolated starless cores and YSOs are found in the north, surrounded by the extinction core associated with L1689N.

In addition to L1689 and L1709, two tight groups of YSOs are found that do not have associated SCUBA cores. One, L1688-N, is found just north of the L1688 cluster, but is not connected directly to the main cluster through strong extinction or ^{13}CO emission in the maps of Loren (1989). The other association is located toward the west of the cloud complex where Loren (1989) found a number of smaller CO clouds. The YSO volume density in this region peaks at the location of the [L89] R12 core: Loren found that this particular core together with another, [L89] R7, showed spatially compact ^{13}CO emission and strong ^{13}CO peaks suggesting that star formation is ongoing. Whereas [L89] R7 does not show up as a separate group in the YSO density maps, it is associated with a high level of extinction $A_V > 10$ and contains a small number of Spitzer identified YSOs. Both the [L89] R12 and L1688-N regions have very low levels of extinction, $\langle A_V \rangle \approx 4$ compared to L1709, L1689 and L1688 where the average extinction is $\langle A_V \rangle = 10 - 15$.

Of the remaining 9 SCUBA cores located outside the boundaries of the L1688, L1689 and L1709 tight groups, seven are associated with the larger loose “e-Oph” association and two are located within the extended cloud where the YSO volume density is lower than $1 M_{\odot} \text{pc}^{-3}$.

4.2.2. *Substructure of Perseus*

Perseus shows a larger variety of structure than Ophiuchus with the regions around the two main clusters, NGC 1333 and IC 348, containing about 80% of the YSOs but only about 55% of those associated with SCUBA cores. This in itself suggests that significant current star formation is going on outside the two main clusters. In contrast to Ophiuchus, the YSO associations in Perseus can be traced to lower levels of volume densities. At the $1 \times \text{LL03}$ level five loose associations of YSOs are identified, connected to the two main clusters, NGC 1333 and IC 348, and the three small groups, B1, L1455 and L1448.

At the $1 \times \text{LL03}$ level the B1 group extends south along the main ridge seen in the extinction and (sub)millimeter emission maps, and encompasses the regions around the deeply embedded YSOs, IRAS 03285+3035 and IRAS 03292+3039 as well as the aggregate of YSOs in the Per 6 region (Rebull et al. 2007).

Each of the loose regions can also be traced to the higher $25 \times \text{LL03}$ level. At this level only e-IC 348 breaks up into multiple tight associations: the main cluster, IC 348, and the smaller group to the southwest, IC 348-SW (Cambr esy et al.). The main IC 348 tight cluster contains all of the SCUBA cores within the loose boundary. As pointed out by Muench et al. (2007) these cores are all located toward the southwest, where the extinction peaks. The association of YSOs in L1448 only has three members at the $25 \times \text{LL03}$ level and is therefore not counted as a tight group.

The other regions each contain one tight cluster or group within their $1 \times \text{LL03}$ levels. NGC 1333 contains close to half of the SCUBA cores in the Perseus cloud, with 85% of the cores within the loose cluster also within the boundaries of the tight cluster. The number of YSOs within the tight groups of IC 348 and NGC 1333 are almost the same (121 and 102, respectively) as are the masses from the extinction maps (318 and 319 M_{\odot}). There is, however, more than a factor 3 difference between the number of Class I objects in these regions, as also noted by J orgensen et al. (2006).

4.3. Key numbers for Perseus and Ophiuchus

Table 6 summarizes the key numbers for each of the regions in Ophiuchus and Perseus. We are here concerned with properties directly related to the current/ongoing star formation status of each region and refer to future papers for further discussion about the more evolved YSOs and overviews of the full YSO populations. In addition to the number of cores, the total core mass, and the number of embedded YSOs from this paper within each region, we also tabulate the number of YSOs from the c2d catalogs (Evans et al. 2007) together with the number of Class I sources. We also calculate two estimates of the star formation efficiency, $SFE = \frac{M_{\text{YSO}}}{M_{\text{gas+dust}} + M_{\text{YSO}}}$, where M_{YSO} is the total mass of YSOs and $M_{\text{gas+dust}}$ is the mass of gas and dust in the considered region. The “core SFE” (SFE_{core}) is calculated on basis of the number of embedded YSOs from this paper and where $M_{\text{gas+dust}}$ is the total mass in SCUBA cores. The other estimate, the “cloud SFE” (SFE_{cloud}), is calculated using the total number of YSOs from the c2d list (i.e., including the more evolved YSOs as well as the embedded YSOs from this paper) and with $M_{\text{gas+dust}}$ being the mass within the considered region (e.g., within a given volume density contour) based on the c2d extinction maps (Evans et al. 2007) and using the conversion between extinction and hydrogen column density, $N_{\text{H}_2} = 9.4 \times 10^{20} \text{cm}^{-2} (A_V/\text{mag})$, from the Copernicus results of Bohlin et al. (1978). The “core SFE” is a measure of how efficient stars form from existing cores with central densities higher than about $5 \times 10^4 \text{cm}^{-3}$ corresponding to the detection limit of the SCUBA data, but does not take into account the YSOs that have already been formed and additional cores which may still form within the cloud. In contrast, the cloud SFE measures how efficient the cloud has been in turning dust and gas into YSOs up to this point in time. For both measures of the SFE we assume a mean stellar mass of $0.5 M_{\odot}$.

Table 6: Key numbers for Ophiuchus and Perseus.

	#YSOs	#Class I ^a	#Cores	#Cores w/MIPS	$\langle A_V \rangle^b$ [mag]	Volume [pc ³]	M_{cloud}^c [M_{\odot}]	M_{core}^d [M_{\odot}]	M_{starless} [M_{\odot}]	SFE _{core}	SFE _{cloud}
Ophiuchus											
Total	290	32 (11%)	66	23 (35%)	3586	74	45	13%	3.9%
e-Oph	266	30 (11%)	64	22 (34%)	5.7	75	2570	74	45	13%	4.9%
L1688	154	20 (13%)	47	19 (40%)	18.1	2.1	742	57	36	14%	9.4%
L1709	8	0 (0.0%)	3	1 (33%)	9.6	0.071	42	0.62	0.36	45%	8.7%
L1689	11	3 (27%)	7	1 (14%)	14.9	0.091	77	4.0	3.9	11%	6.7%
[L89] R12	7	1 (14%)	0	...	4.5	0.054	16	0.0	18%
L1688-N	7	0 (0.0%)	0	...	4.1	0.067	17	0.0	17%
other	79	6 (6.6%)	7	1 (14%)	1686	12	4.6	4.0%	2.2%
DC1d 356.1	5	2 (40%)	0	...	2.4	0.36	31	0.0	7.5%
Extended	19	0 (0.0%)	2	1 (50%)	985	0.69	0.66	7.2%	0.96%
Perseus											
Total	385	89 (23%)	72	42 (58%)	7080	106	24	17%	2.6%
e-NGC1333	115	41 (36%)	33	20 (61%)	6.2	12	822	55	11	15%	6.5%
NGC1333	102	35 (34%)	28	16 (57%)	12.7	0.98	319	53	10	13%	14%
other	13	6 (46%)	5	4 (80%)	502	1.8	0.54	53%	1.3%
e-IC348	189	15 (7.9%)	12	4 (33%)	6.2	33	1611	14	5.0	13%	5.5%
IC348	121	11 (9.1%)	12	4 (33%)	8.1	1.9	318	14	5.0	13%	16%
IC348-SW	10	2 (20%)	0	...	11.8	0.086	59	0.0	7.8%
other	58	2 (3.4%)	0	1234	0.0	2.3%
e-B1	34	14 (41%)	10	7 (70%)	5.9	15	919	15	2.0	25%	1.8%
B1	9	8 (89%)	7	5 (71%)	17.5	0.075	79	13	0.84	16%	5.4%
other	25	6 (24%)	3	2 (67%)	840	2.4	1.0	30%	1.5%
e-L1455	8	6 (75%)	5	5 (80%)	5.3	1.9	211	3.1	0.55	39%	1.8%
L1455	5	5 (100%)	5	5 (80%)	8.1	0.035	22	3.1	0.55	39%	10%
other	3	1 (33%)	0	189	0.0	0.79%
L1448	5	5 (100%)	6	3 (50%)	4.6	1.4	147	16	5.4	8.5%	1.7%
Extended	34	8 (24%)	6	4 (67%)	3371	3.6	0.55	36%	0.52%

^aNumber of Class I YSOs and fraction of the total number of YSOs in the given region.^bAverage A_V from the extinction maps within the volume density contour used to define the given region.^cTotal mass within the given volume density contour from the c2d extinction map.^dTotal mass of the SCUBA cores located within the given volume density contour.

4.4. Perseus vs. Ophiuchus: fraction of embedded sources and SFE

In contrast to Ophiuchus, the Perseus regions show large variety in the relative numbers of embedded YSOs - both when defined as being associated with submillimeter cores or based on their mid-infrared spectral index (i.e., the classical definition of Class I YSOs). The difference between IC 348 and the collection of groups including NGC 1333, L1455, L1448 and B1 was also discussed by Jørgensen et al. (2006). The smaller groups contain only 20% of the YSOs in the entire Perseus complex but about 40% of both the Class I sources and the MIPS sources associated with submillimeter cores. In the central tight, B1, L1455 and L1448, groups, the ratios of Class I sources to total YSOs are in fact 90–100% compared to 34% in NGC 1333 and 10–20% in the two tight clusters/groups in IC 348. In the more extended regions around these tight groups the ratios of Class Is to total YSOs are, in contrast, much lower. For example, in B1 the loose group further south in the extinction ridge and the Per 6 aggregate have about 25% Class I sources. The ratio of Class I YSOs in the Ophiuchus groups is more similar to that of IC 348 than those of the smaller groups and NGC 1333.

Another property which is interesting to compare is the star formation efficiency, SFE (see §4.3). As discussed in Jørgensen et al. (2007) it is convenient to distinguish between the “core” star formation efficiency, SFE_{core} , and “cloud” star formation efficiency, SFE_{cloud} : SFE_{core} is based on the masses of the embedded YSOs in the cloud compared to the mass of the dust and gas already collected in dense cores. It is therefore a good measure of the star formation efficiency for the current generation of dense cores but does not take into account those stars which have evolved away from the embedded stages or those cores which may still form from gas within the cloud. SFE_{cloud} in contrast is based on the masses of all (identified) YSOs in the studied region and the total mass based on extinction maps (i.e., mass in the extended cloud at lower column densities) and therefore captures the star formation efficiency over the larger time-span corresponding to the evolution of the YSOs from the formation of the cores through the YSO Class 0–II stages. The biggest caveats about these definitions are (1) the completeness of the YSO samples (large number of diskless YSOs may for example remain undefined by the photometric surveys because they have too little dust emission to show significant infrared excesses) and (2) that dust and gas in the cloud might disperse over the timescale during which the YSOs evolve.

For the regions in Perseus and Ophiuchus, values of SFE_{core} are 10–30% - with no significant differences between the two clouds. For SFE_{cloud} , the average number for Perseus (2.6%) is only slightly lower than in Ophiuchus (4.1%). When individual regions are considered, however, a more pronounced difference is found: the two clusters and the Ophiuchus region show SFE_{cloud} values of about 6% whereas the more isolated groups show lower effi-

ciencies of about 2% (at the $1 \times LL03$ level). For the tight groups and clusters, the regions in Ophiuchus - except L1689 - and NGC 1333 and IC 348, also show higher efficiencies than do the smaller regions of Perseus. These differences can be interpreted in two ways: one possibility is that there is a continuous replenishment of material in the dense cores and the higher SFE_{cloud} of the larger regions simply reflect that these are more effective in turning dust and gas into new stars. A different explanation is that the smaller regions in Perseus only recently have started forming stars and therefore show a lower SFE_{cloud} than the larger clouds. We will return to this discussion in §5.

5. Discussion: Evolution of embedded protostars

The differences between Perseus and Ophiuchus in the numbers of embedded protostars are interesting in the context of the evolution of YSOs through their earliest stages - and suggests evolutionary differences between the two clouds related to differences either in the evolution of individual YSOs or the star formation complex as a whole. To reiterate, compared to Perseus, the regions in Ophiuchus show:

1. a lower fraction of Class I sources compared to the total number of YSOs
2. a lower fraction of MIPS sources associated with SCUBA cores
3. fewer “red” ($[3.6] - [4.5] > 1$ and $[8.0] - [24] > 4.5$) sources from the comparison of the SCUBA cores and MIPS sources from this paper and Jørgensen et al. (2007)

The differences between the number of sources in these different classes raise concerns about timescales for the evolution of prestellar cores and protostars derived on basis of for example the relative numbers of starless and starforming cores or the number of Class I vs. II sources. In terms of star formation efficiencies, the central Ophiuchus region(s) and the two clusters in Perseus, IC 348 and NGC 1333, show higher cloud star formation efficiencies than L1689 in Ophiuchus and the smaller L1455, L1448 and B1 groups in Perseus.

5.1. Difference in evolutionary stages?

One explanation for the differences between the number of embedded sources in Ophiuchus and Perseus might be that the clouds have different “ages”. If star formation has initiated (e.g., been triggered) at a given time in the recent past of the cloud history and the

embedded YSOs evolve on similar timescales the lower number of embedded sources in Ophiuchus suggest that this cloud is more evolved compared to Perseus. A similar effect has been observed within Perseus with clear differences in the numbers of embedded YSOs in IC 348 and NGC 1333 (Jørgensen et al. 2006) in line with the different age estimates for the two clusters of about 2 Myr (Luhman et al. 2003) and < 1 Myr (Lada et al. 1996; Wilking et al. 2004), respectively. The difference in SFE_{cloud} between Ophiuchus and Perseus could then simply reflect that a smaller amount of the dust and gas has turned into stars at this point of the evolution of Perseus. In principle, there is no reason why star formation in Perseus and Ophiuchus should have initiated at the same time, so from that perspective this is definitely a plausible scenario.

What does complicate the picture of a pure evolutionary effect are the relative numbers of SCUBA cores with and without associated MIPS sources (or protostellar and starless cores, respectively). As pointed out above, the small groups in Perseus show very high numbers of Class I sources corresponding to 90–100% of the YSOs in the groups, but these regions do not have the same high fractions of associated MIPS sources. This is naturally explained if B1, L1448 and L1455 have all only recently started forming stars and therefore not all of their cores have yet collapsed. The issue with this interpretation is that Ophiuchus also shows a low fraction of cores with embedded protostars relative to the total number of cores. In a scenario where the time for the initiation star formation differs, the relatively high number of starless cores in Ophiuchus would therefore mean that these remaining starless cores either are “fizzles” (i.e., did not “manage” to collapse) - or that a second generation of star formation is about to occur in this cloud. Nutter et al. (2006) argued that the differences seen between L1689 and L1688 - the latter having a more active star formation history - could be attributed to sequential star formation triggered by a small group of young high mass stars, σ Sco, in the Sco-Cen association.

5.2. Difference in star formation physics?

Another possible explanation for the differences between the regions in Perseus and Ophiuchus is that the physics regulating the star formation between these regions differ, e.g., the time-scale for evolution through the embedded stages is different in the dense clusters in Perseus and in Ophiuchus compared to the more isolated groups. If the collapse of an ensemble of cores occurs stochastically over a time-scale which is long compared to the collapse time for an individual core, the ratio of sources in different evolutionary stages can be used as a statistical tool for measuring the relative durations of star formation phases. Thus, if the collapse of cores occurs slower (or the rate is lower) or if the timescale for evolution

through the embedded stages is shorter - more Class 0/I sources would have time to evolve away from the embedded stages skewing the statistics toward more evolved (Class II) YSOs. Such a solution could explain the undercounting of embedded sources in Ophiuchus as a whole but does not explain the higher SFE_{cloud} in Ophiuchus and NGC 1333 and IC 348.

What could be the physical explanations for such a difference? As pointed out by Jayawardhana et al. (2001) pre-stellar cores and protostars formed in more dense star-forming regions are likely to have high masses on small scales, which in turn will imply high accretion rates, e.g., compared to objects in less dense regions such as Taurus. If this is the case, one would therefore expect that the Ophiuchus protostars were found in regions with higher extinction (and thus further evolved) than those in Perseus. If one compares the major clusters in the two clouds, there does seem to be such a trend with L1688 and L1689 having an average extinction of 15–17 compared to the 8–13 for IC 348 and NGC 1333. This would in turn require that the current population of embedded protostars in Perseus have lower accretion rates than those few sources observed in Ophiuchus. Other factors, such as differences in the global and local magnetic field strengths between Perseus and Ophiuchus, could of course also be important in this context, although no strong observational constraints exist.

5.3. Difference in definitions?

A final explanation for the differences between Ophiuchus and Perseus could simply be that the empirical evolutionary classification scheme does not apply well to comparisons across clouds. For example, it is important to realize the difference between the mid-infrared and submillimeter observations: where the latter measures the dust (plus gas) mass, M , and core temperature, the former measures the extinction or line of sight column density, N , - and thus mid-infrared “redness” - of the central star+disk system. If one just takes a spherical symmetric envelope with a density profile, $n \propto r^{-p}$ and inner and outer radii, R_{in} and R_{out} , it is easily seen that:

$$M \propto \int_{R_{\text{in}}}^{R_{\text{out}}} n(r) 4\pi r^2 dr \propto \int_{R_{\text{in}}}^{R_{\text{out}}} r^{2-p} dr \propto R_{\text{out}}^{3-p} - R_{\text{in}}^{3-p} \approx R_{\text{out}}^{3-p} \quad (5)$$

$$N \propto \int_{R_{\text{in}}}^{R_{\text{out}}} n(r) dr \propto \int_{R_{\text{in}}}^{R_{\text{out}}} r^{-p} dr \propto R_{\text{out}}^{1-p} - R_{\text{in}}^{1-p} \approx R_{\text{in}}^{1-p} \quad (6)$$

when $R_{\text{out}} \gg R_{\text{in}}$ and $1.0 < p < 3.0$. That is, a larger inner radius decreases the extinction of a given protostellar source (e.g., making it visible at shorter wavelengths (Jørgensen et al. 2005) or reducing its “redness”) while not affecting the envelope mass and vice versa: a larger outer radius only increases the envelope mass and thus submillimeter flux, but does not affect the mid-infrared signature of the source. If the inner radius or flattening of the protostellar

envelopes in Ophiuchus is larger than that in Perseus the protostars there will appear more evolved if classified based on their mid-infrared colors or α . This could for example be the case if the angular momenta of the pre-stellar cores had been different, resulting in larger centrifugal radii for the sources in Ophiuchus. The difference in the maximum redness in Perseus and Ophiuchus (§3.1) could be taken as evidence that such an effect is in play.

The bottom line is that based on the current data it is difficult to say which scenario is most likely; indeed, a combination very likely applies. Regardless, challenges are brought to the definition of the most deeply embedded stages of low-mass protostars, i.e., Class 0 stage. It is here useful to remind of the three definitions of Class 0 sources (see André et al. 1993, 2000): the conceptional definition of the Class 0 stage is that the protostar has accreted less than half its final mass, but since it is difficult to determine the masses of the central protostars, this definition is not useful for practical purposes. Two main observational definitions are in play: most often that the object emit most of its luminosity at submillimeter wavelength (either quantified by a ratio of the submillimeter luminosity to total luminosity, $L_{\lambda \geq 350\mu\text{m}}/L_{\text{bol}} > 0.5\%$ or a bolometric temperature lower than 70–100 K) - or that it has a high mass accretion rate or equivalently drives a powerful outflow.

The main issue is that taken separately, the Ophiuchus and Perseus data provide very different arguments for the life-time of the Class 0 stage. Assuming a constant birthrate, the relatively large number of embedded YSOs in Perseus compared to more evolved YSOs suggests that the Class 0 stage is not simply a short-lived, high accretion stage. This is in direct contrast to the conclusion derived from the Ophiuchus YSO sample, where the deeply embedded sources are significantly outnumbered, requiring a very short-lived Class 0 phase. A reasonable solution to this discrepancy may be that differences between the appearance of the YSOs reflects strongly their environments (physical conditions). In this case, Class 0 protostars may not represent a clearly defined early stage in the evolution of protostars but rather, an environmentally affected, continuum into Class I protostars (as also discussed by Jayawardhana et al. (2001)). An alternative explanation, that star formation occurs in bursts, could explain the differences if the most recent burst in Perseus has occurred more recently than that in Ophiuchus. In this case, however, the relative number of embedded versus more evolved YSOs does not reveal their relative time-scales and thus do not provide the evidence that the time-scale for the evolution through the most deeply embedded Class 0 stage is significantly shorter than the evolution through the Class I stage.

6. Summary

We have combined SCUBA submillimeter dust continuum and Spitzer mid-IR surveys of the current star formation in the Ophiuchus cloud complex. The results are compared to our previous study of Perseus. The main conclusions of this study are as follows:

- We have applied a method developed for identifying embedded protostars in Perseus (Jørgensen et al. 2007) directly to the Ophiuchus datasets.
- Little dispersal of the protostars with respect to the SCUBA cores are seen similar to the situation in Perseus. Fewer red sources are found in Ophiuchus compared to Perseus - but also a higher fraction of starless SCUBA cores.
- Although distance does not directly play into the definition of SCUBA cores, the Ophiuchus surveys are more sensitive to dust emission from disks, representing a small, but non-negligible fraction of the sources seen in the SCUBA survey.
- As was the case in Perseus most of the SCUBA cores in Ophiuchus with high concentrations also have associated MIPS sources, likely reflecting the heating of the dust from the central source making them appear more peaked. Four high concentration SCUBA cores without associated YSOs are identified and are found to be the likely result of the impact of outflow and the structure of the ambient environment.
- Using a nearest-neighbor algorithm we calculate surface and volume densities of the YSOs in Perseus and Ophiuchus and from those identify groups and clusters in each of the clouds. For each of these regions we calculate key numbers such as masses, star formation efficiencies and the fraction of embedded objects.
- The star formation efficiency varies across and within clouds. Perseus has a high efficiency in turning material from the SCUBA cores into embedded protostars (a high SFE_{core}), driven primarily by the efficiency in its smaller groups (B1, L1455 and L1448). The large clusters in Perseus (NGC 1333 and IC 348) have lower core SFEs, similar to those found across Ophiuchus. The cloud SFE measured on basis of the larger scale dust extinction and the overall population of YSOs, however, is somewhat higher in Ophiuchus than in Perseus primarily because these same small groups in Perseus (B1, L1455 and L1448) have a larger fraction of their mass still not turned into cores or stars. Generally, though the cloud SFE is lower than the core SFE, suggesting that the star formation mechanism is more inefficient on larger relative to smaller scales. The fraction of Class I sources relative to YSOs also vary from about 10% in Ophiuchus and IC 348 to 35% in NGC 1333 and more than 90% in the inner

regions of B1, L1455 and L1448. Finally, the fraction of starless cores in Ophiuchus is found to be high compared to in Perseus.

- We discuss possible explanations for the differences between the regions in Perseus and Ophiuchus, such as (i) that the YSOs have evolved over different timescales, (ii) that the physics regulating the star formation, e.g., the accretion in the two clouds, differ, or (iii) that the empirical evolutionary classification scheme does not apply well when comparing samples of YSOs from different clouds. Based on the existing samples it is not possible to rule out any of these scenarios, and likely all three may be relevant for the full picture of the star formation properties of the two clouds. In any case, the results do raise questions about the standard picture of the Class 0 stage being a short-lived precursor to the Class I stage in the evolution of embedded YSOs.

The results presented here provide a direct comparison of the global star formation properties of the larger scale clouds and also provides important constraints on - and raises questions about - the general low-mass star formation scenario. It demonstrates the importance of the systematic approach using the large scale maps which are currently appearing from Spitzer and the new submillimeter cameras, LABOCA on APEX and SCUBA-2 on the JCMT. Together these surveys can address whether differences between the number of sources in the embedded stages are generally seen or, e.g., whether Perseus or Ophiuchus contain YSO populations “more representative” for other regions currently forming stars. Other complementary observations (e.g., large scale submillimeter line maps) can address whether differences in the initial conditions (e.g., pressure or turbulence) could be responsible for the observed differences in the YSO populations. At the same time these large-scale surveys are providing important unbiased samples of embedded low-mass protostars that will be obvious targets for detailed observations with upcoming facilities such as ALMA.

We are grateful to Rob Gutermuth, Neal Evans, Melissa Enoch, and Jens Kauffmann for helpful discussions and comments about the paper. We also thank the referee, Bruce Wilking, for insightful comments that improved the paper. D.J. is supported by a Natural Sciences and Engineering Research Council of Canada grant. H.K. is supported by a Natural Sciences and Engineering Research Council of Canada CGS Award and a National Research Council of Canada GSSSP Award. This paper has made use of the SIMBAD database, operated at CDS, Strasbourg, France.

A. Properties of submillimeter cores.

We here present the list of submillimeter cores in Ophiuchus. See Johnstone et al. (2004) for further details about the observations and Kirk et al. (2006) for further discussion about the algorithm for identifying cores and their properties.

Table 7. Properties of submillimeter cores in Ophiuchus

Name ^a (SMM J)	R.A. ^b (J2000)	Decl. ^b (J2000)	f_0^c (Jy beam ⁻¹)	S_{850}^c (Jy)	R_{eff}^c (arcsec)	Mass ^d (M_\odot)	Concentration	Temperature ^e (K)	M_{BE}^e (M_\odot)	$\log n_{\text{cent}}^e$ (cm ⁻³)	$\log P_{\text{ext}}/k^e$ (cm ⁻³ K ⁻¹)
162608-24202	16 26 08.0	-24 20 24.5	0.31	3.32	38	0.76	0.34	24	0.40	4.8	6.1
162610-24195	16 26 09.6	-24 19 45.5	0.30	2.11	31	0.48	0.34	21	0.29	5.0	6.2
162610-24231	16 26 10.2	-24 23 09.5	0.29	1.94	31	0.44	0.40	16	0.40	5.1	6.2
162610-24206	16 26 10.4	-24 20 57.5	0.45	3.50	44	0.80	0.65	11	1.3	5.7	5.8
162614-24232	16 26 13.9	-24 23 24.6	0.20	0.58	17	0.13	0.15	16	0.13	5.3	6.5
162614-24234	16 26 13.9	-24 23 42.6	0.20	1.10	25	0.25	0.22	17	0.20	5.1	6.2
162614-24250	16 26 14.4	-24 25 00.6	0.28	5.93	53	1.4	0.34	25	0.62	4.6	5.9
162615-24231	16 26 14.6	-24 23 06.6	0.20	2.16	34	0.49	0.17	20	0.31	4.9	6.1
162616-24235	16 26 15.7	-24 23 54.7	0.20	1.03	24	0.23	0.20	17	0.19	5.1	6.3
162617-24235	16 26 17.5	-24 23 45.7	0.29	3.93	42	0.89	0.32	23	0.45	4.8	6.0
162622-24225	16 26 21.6	-24 22 54.8	0.82	13.2	58	3.0	0.58	17	2.4	5.4	6.0
162624-24162	16 26 24.1	-24 16 15.9	0.45	0.27	10	0.06	0.41	12	0.10	6.1	7.0
162626-24243	16 26 26.5	-24 24 30.9	3.23	32.2	66	7.3	0.80	22	4.1	5.8	6.0
162627-24233	16 26 27.3	-24 23 33.9	3.35	13.3	32	3.0	0.66	21	1.8	6.2	6.7
162628-24235	16 26 27.5	-24 23 54.9	4.22	33.3	59	7.6	0.80	23	3.9	6.0	6.2
162628-24225	16 26 28.0	-24 22 54.9	1.11	21.0	70	4.8	0.66	18	3.4	5.5	5.9
162633-24261	16 26 32.8	-24 26 13.0	0.45	30.0	100	6.8	0.41	29	2.6	4.4	5.7
162641-24272	16 26 40.5	-24 27 16.1	0.34	3.72	45	0.85	0.53	13	1.1	5.3	5.9
162644-24173	16 26 43.6	-24 17 28.2	0.35	0.95	20	0.22	0.40	14	0.24	5.5	6.5
162644-24345	16 26 44.4	-24 34 49.2	0.24	0.19	10	0.04	0.29	13	0.06	5.8	6.8
162644-24253	16 26 44.5	-24 25 28.2	0.21	1.81	31	0.41	0.23	19	0.28	4.9	6.1
162645-24231	16 26 45.1	-24 23 10.2	0.67	3.06	39	0.70	0.74	11	1.2	6.0	5.9
162646-24242	16 26 46.0	-24 24 19.2	0.20	1.74	30	0.40	0.16	19	0.27	5.0	6.1
162648-24236	16 26 47.5	-24 23 55.2	0.23	2.25	36	0.51	0.33	20	0.33	4.8	6.0
162659-24454	16 26 58.7	-24 45 37.3	0.40	0.35	12	0.08	0.42	12	0.13	6.0	6.8
162660-24343	16 26 59.6	-24 34 25.3	0.59	16.0	73	3.6	0.55	18	2.8	5.1	5.8
162705-24363	16 27 05.3	-24 36 28.4	0.25	0.37	14	0.08	0.34	14	0.09	5.5	6.6

Table 7—Continued

Name ^a (SMM J)	R.A. ^b (J2000)	Decl. ^b (J2000)	f_0^c (Jy beam ⁻¹)	S_{850}^c (Jy)	R_{eff}^c (arcsec)	Mass ^d (M_\odot)	Concentration	Temperature ^e (K)	M_{BE}^e (M_\odot)	$\log n_{\text{cent}}^e$ (cm ⁻³)	$\log P_{\text{ext}}/k^e$ (cm ⁻³ K ⁻¹)
162705-24391	16 27 05.3	-24 39 13.4	0.35	2.31	32	0.53	0.44	14	0.58	5.3	6.2
162707-24381	16 27 07.1	-24 38 13.4	0.20	0.18	10	0.04	0.22	12	0.06	5.7	6.7
162709-24372	16 27 09.5	-24 37 19.4	0.36	0.83	20	0.19	0.48	11	0.34	5.8	6.5
162711-24393	16 27 10.8	-24 39 25.4	0.22	0.90	23	0.21	0.29	17	0.17	5.2	6.3
162712-24290	16 27 11.7	-24 29 04.4	0.21	0.50	16	0.11	0.21	15	0.11	5.4	6.5
162712-24380	16 27 12.1	-24 38 01.4	0.22	0.53	18	0.12	0.31	15	0.12	5.3	6.4
162713-24295	16 27 12.6	-24 29 49.4	0.32	1.28	24	0.29	0.38	18	0.23	5.2	6.3
162715-24303	16 27 14.8	-24 30 25.4	0.25	0.99	23	0.22	0.34	17	0.18	5.2	6.3
162725-24273	16 27 25.1	-24 27 28.4	0.46	3.09	31	0.70	0.37	24	0.34	5.1	6.3
162727-24405	16 27 26.7	-24 40 52.3	0.57	16.0	76	3.6	0.57	17	3.0	5.1	5.7
162728-24271	16 27 28.0	-24 27 10.3	0.66	4.26	30	0.97	0.34	28	0.38	5.2	6.5
162728-24393	16 27 28.0	-24 39 34.3	0.27	0.74	20	0.17	0.37	16	0.15	5.3	6.4
162729-24274	16 27 29.5	-24 27 40.3	0.47	2.50	31	0.57	0.50	13	0.70	5.6	6.3
162730-24264	16 27 29.7	-24 26 37.3	0.44	2.23	26	0.51	0.35	22	0.27	5.2	6.4
162730-24415	16 27 30.2	-24 41 49.3	0.22	2.69	40	0.61	0.32	20	0.38	4.8	6.0
162733-24262	16 27 33.0	-24 26 22.3	0.52	4.68	38	1.1	0.45	17	0.87	5.3	6.2
162739-24424	16 27 38.8	-24 42 37.2	0.22	1.64	31	0.37	0.31	19	0.26	4.9	6.1
162740-24431	16 27 39.9	-24 43 13.2	0.20	0.56	18	0.13	0.27	15	0.13	5.3	6.4
162759-24334	16 27 58.5	-24 33 43.0	0.36	2.78	35	0.63	0.46	14	0.69	5.3	6.1
162821-24362	16 28 21.4	-24 36 24.5	0.29	0.73	19	0.17	0.39	14	0.18	5.4	6.4
163133-24032	16 31 32.5	-24 03 15.9	0.23	1.63	31	0.23	0.35	17	0.19	5.1	6.2
163136-24013	16 31 35.8	-24 01 28.0	0.86	1.85	26	0.26	0.72	10	0.57	6.5	6.3
163138-24495	16 31 38.2	-24 49 47.7	0.39	4.89	42	1.1	0.38	24	0.56	4.9	6.1
163139-24506	16 31 38.9	-24 50 59.7	0.22	2.11	36	0.48	0.35	19	0.32	4.8	6.0
163140-24485	16 31 40.5	-24 48 53.8	0.21	1.03	25	0.24	0.29	17	0.19	5.1	6.2
163141-24495	16 31 41.3	-24 49 47.8	0.35	3.93	40	0.89	0.36	24	0.44	4.8	6.1
163143-24003	16 31 43.3	-24 00 28.2	0.24	0.94	23	0.13	0.33	15	0.13	5.3	6.4

Table 7—Continued

Name ^a (SMM J)	R.A. ^b (J2000)	Decl. ^b (J2000)	f_0^c (Jy beam ⁻¹)	S_{850}^c (Jy)	R_{eff}^c (arcsec)	Mass ^d (M_\odot)	Concentration	Temperature ^e (K)	M_{BE}^e (M_\odot)	$\log n_{\text{cent}}^e$ (cm ⁻³)	$\log P_{\text{ext}}/k^e$ (cm ⁻³ K ⁻¹)
163154-24560	16 31 53.8	-24 56 00.2	0.27	1.87	32	0.43	0.40	15	0.41	5.1	6.1
163157-24572	16 31 57.1	-24 57 18.4	0.30	3.43	43	0.78	0.46	14	0.87	5.2	6.0
163201-24564	16 32 00.9	-24 56 42.5	0.36	0.33	12	0.08	0.45	10	0.16	6.0	6.8
163223-24284	16 32 22.9	-24 28 37.1	14.57	33.27	56	7.6	0.94	24	3.8	6.0	6.2
163229-24291	16 32 29.1	-24 29 07.2	1.34	16.19	64	3.7	0.74	17	3.1	5.7	5.8
163230-23556	16 32 29.7	-23 55 55.6	0.26	1.46	27	0.20	0.33	17	0.17	5.2	6.4
163247-23524	16 32 47.0	-23 52 43.5	0.23	2.36	35	0.33	0.26	19	0.23	5.0	6.2
163248-23524	16 32 48.0	-23 52 40.5	0.22	0.61	19	0.08	0.30	14	0.09	5.5	6.5
163248-23523	16 32 48.3	-23 52 25.5	0.21	0.53	17	0.07	0.19	14	0.08	5.6	6.6
163249-23521	16 32 49.3	-23 52 13.5	0.22	0.99	24	0.14	0.28	16	0.13	5.3	6.4
163356-24420	16 33 55.7	-24 42 04.3	0.20	0.12	9	0.03	0.33	11	0.05	5.8	6.8
163448-24381	16 34 48.5	-24 38 05.8	0.24	2.91	42	0.66	0.38	19	0.47	4.8	6.0

Note. — Units of right ascension are hours, minutes, and seconds, and units of declination are degrees, arcminutes, and arcseconds.

^aName formed from J2000.0 positions.

^bPosition of peak flux within clump (accurate to 3''; the pixel size in the SCUBA maps and the approximate pointing accuracy of the JCMT).

^cPeak flux, total flux, and outer radius derived from Clumfind (Williams et al. 1994). The peak and total fluxes have uncertainties of about 20%, mostly due to uncertainties in the absolute flux calibration. The radius has not been deconvolved from the telescope beam.

^dMass derived from the total flux assuming $T_d = 15$ K and $850 \text{ cm}^2 \text{ g}^{-1}$, $d = 125$ pc.

^eConcentration, temperature, mass, central number density, and external pressure derived from Bonnor-Ebert modeling (see text).

REFERENCES

- Allen, L. E., et al. 2008, ApJ, in prep.
- André, P., Ward-Thompson, D., & Barsony, M. 1993, ApJ, 406, 122
- André, P., Ward-Thompson, D., & Barsony, M. 2000, in Protostars and Planets IV, ed. V. Mannings, A. P. Boss, & S. S. Russell (University of Arizona Press, Tucson), 59
- Andrews, S. M., & Williams, J. P. 2005, ApJ, 631, 1134
- Bergin, E. A., Ciardi, D. R., Lada, C. J., Alves, J., & Lada, E. A. 2001, ApJ, 557, 209
- Bohlin, R. C., Savage, B. D., & Drake, J. F. 1978, ApJ, 224, 132
- Bontemps, S., et al. 2001, A&A, 372, 173
- Cambrésy, L., Petropoulou, V., Kontizas, M., & Kontizas, E. 2006, A&A, 445, 999
- Casertano, S., & Hut, P. 1985, ApJ, 298, 80
- Castets, A., Ceccarelli, C., Loinard, L., Caux, E., & Leffloch, B. 2001, A&A, 375, 40
- Chandler, C. J., & Richer, J. S. 2000, ApJ, 530, 851
- de Geus, E. J., de Zeeuw, P. T., & Lub, J. 1989, A&A, 216, 44
- Di Francesco, J., André, P., & Myers, P. C. 2004, ApJ, 617, 425
- Di Francesco, J., Johnstone, D., Kirk, H., MacKenzie, T., & Ledwosinska, E. 2008, ApJS, in press. (ArXiv: 0801.2595)
- Enoch, M., et al. 2008, ApJ, in prep.
- Enoch, M. L., et al. 2006, ApJ, 638, 293
- Evans, N. J., et al. 2003, PASP, 115, 965
- Evans, N. J., et al. 2007, "Final Delivery of Data from the c2d Legacy Project: IRAC and MIPS (Pasadena, SSC)"
- Feitzinger, J. V., & Stuewe, J. A. 1984, A&AS, 58, 365
- Geers, V. C., Pontoppidan, K. M., van Dishoeck, E. F., Dullemond, C. P., Augereau, J.-C., Merín, B., Oliveira, I., & Pel, J. W. 2007, A&A, 469, L35

- Goodman, A. A., et al. 2004, ASP Conference Series
- Greene, T. P., Wilking, B. A., Andre, P., Young, E. T., & Lada, C. J. 1994, ApJ, 434, 614
- Gutermuth, R. A., Megeath, S. T., Pipher, J. L., Williams, J. P., Allen, L. E., Myers, P. C., & Raines, S. N. 2005, ApJ, 632, 397
- Gutermuth, R. A., et al. 2008, ApJ in press., ArXiv: 0710.1860
- Harvey, P., Merín, B., Huard, T. L., Rebull, L. M., Chapman, N., Evans, N. J., II, & Myers, P. C. 2007, ApJ, 663, 1149
- Hatchell, J., Fuller, G. A., Richer, J. S., Harries, T. J., & Ladd, E. F. 2007, A&A, 468, 1009
- Jayawardhana, R., Hartmann, L., & Calvet, N. 2001, ApJ, 548, 310
- Johnstone, D., Di Francesco, J., & Kirk, H. 2004, ApJ, 611, L45
- Johnstone, D., Wilson, C. D., Moriarty-Schieven, G., Giannakopoulou-Creighton, J., & Gregersen, E. 2000a, ApJS, 131, 505
- Johnstone, D., Wilson, C. D., Moriarty-Schieven, G., Joncas, G., Smith, G., Gregersen, E., & Fich, M. 2000b, ApJ, 545, 327
- Jørgensen, J. K., et al. 2006, ApJ, 645, 1246
- Jørgensen, J. K., Johnstone, D., Kirk, H., & Myers, P. C. 2007, ApJ, 656, 293
- Jørgensen, J. K., et al. 2005, ApJ, 631, L77
- Jørgensen, J. K., Schöier, F. L., & van Dishoeck, E. F. 2004, A&A, 416, 603
- Kirk, H., Johnstone, D., & Di Francesco, J. 2006, ApJ, 646, 1009
- Lada, C. J. 1987, in IAU Symp. 115: Star Forming Regions (D. Reidel Publishing Co., Dordrecht), Vol. 115, 1
- Lada, C. J., Alves, J., & Lada, E. A. 1996, AJ, 111, 1964
- Lada, C. J., & Lada, E. A. 2003, ARA&A, 41, 57
- Lahuis, F., et al. 2006, ApJ, 636, L145
- Loren, R. B. 1989, ApJ, 338, 902
- Loren, R. B., Wootten, A., & Wilking, B. A. 1990, ApJ, 365, 269

- Luhman, K. L., Stauffer, J. R., Muench, A. A., Rieke, G. H., Lada, E. A., Bouvier, J., & Lada, C. J. 2003, *ApJ*, 593, 1093
- Mamajek, E. E. 2008, *AN*, in press. (arXiv: 0709.0505)
- Motte, F., André, P., & Neri, R. 1998, *A&A*, 336, 150
- Muench, A. A., Lada, C. J., Luhman, K. L., Muzerolle, J., & Young, E. 2007, *AJ*, 134, 411
- Noriega-Crespo, A., Morris, P., Marleau, F. R., Carey, S., Boogert, A. C. A., van Dishoeck, E. F., Evans, N. J., & Authors, O. 2004, *ApJS*, in press.
- Nutter, D., Ward-Thompson, D., & André, P. 2006, *MNRAS*, 368, 1833
- Padgett, D. L., et al. 2008, *ApJ*, 672, 1013
- Pontoppidan, K. M., Dullemond, C. P., van Dishoeck, E. F., Blake, G. A., Boogert, A. C. A., Evans, N. J., Kessler-Silacci, J. E., & Lahuis, F. 2005, *ApJ*, 622, 463
- Porras, A., et al. 2007, *ApJ*, 656, 493
- Rebull, L. M., et al. 2007, *ApJS*, 171, 447
- Ridge, N. A., et al. 2006, *AJ*, 131, 2921
- Stanke, T., Smith, M. D., Gredel, R., & Khanzadyan, T. 2006, *A&A*, 447, 609
- Stark, R., et al. 2004, *ApJ*, 608, 341
- Struve, O., & Rudkjøbing, M. 1949, *ApJ*, 109, 92
- Stutz, A. M., et al. 2007, *ApJ*, 665, 466
- Visser, A. E., Richer, J. S., & Chandler, C. J. 2002, *AJ*, 124, 2756
- Wilking, B. A., Gagné, M., & Allen, L. E. 2008, in *Handbook of Low Mass Star Forming Regions* (ASP Conference Series; B. Reipurth, ed.)
- Wilking, B. A., Meyer, M. R., Greene, T. P., Mikhail, A., & Carlson, G. 2004, *AJ*, 127, 1131
- Wilking, B. A., Meyer, M. R., Robinson, J. G., & Greene, T. P. 2005, *AJ*, 130, 1733
- Williams, J. P., de Geus, E. J., & Blitz, L. 1994, *ApJ*, 428, 693
- Wilson, C. D., et al. 1999, *ApJ*, 513, L139

Young, K. E., et al. 2006, ApJ, 644, 326